A comprehensive human embryo reference tool using single-cell RNA-sequencing data

Zhao, Cheng; Reyes, Alvaro Plaza; Schell, John Paul; Weltner, Jere; Ortega, Nicolas M. ...

2024-11-14
Nature Research
http://hdl.handle.net/10138/588660
Zhao, C, Reyes, A P, Schell, J P, Weltner, J, Ortega, N M, Zheng, Y, Björklund, Å K, Baque-vidal, L, Sokka, J, Torokovic, R, Cox, B, Rossant, J, Fu, J, Petropoulos, S & Lanner, F 2024, 'A comprehensive human embryo reference tool using single-cell RNA-sequencing data', Nature methods, vol. 22, pp. 193-206. https://doi.org/10.1038/s41592-024-02493-2

nature methods

Resource

https://doi.org/10.1038/s41592-024-02493-2

A comprehensive human embryo reference tool using single-cell RNA-sequencing data

Received: 9 February 2024

Accepted: 30 September 2024

Published online: 14 November 2024

Check for updates

Cheng Zhao[1], Alvaro Plaza Reyes[1,2], John Paul Schell[1], Jere Weltner[1,3,4], Nicolás M. Ortega[1], Yi Zheng[5,6], Åsa K. Björklund[7], Laura Baqué-Vidal[1], Joonas Sokka[3], Ras Torokovic[3], Brian Cox[8], Janet Rossant[9], Jianping Fu[5,10,11], Sophie Petropoulos[1,12,13] ✉ & Fredrik Lanner[1,14] ✉

Stem cell-based embryo models offer unprecedented experimental tools for studying early human development. The usefulness of embryo models hinges on their molecular, cellular and structural fidelities to their in vivo counterparts. To authenticate human embryo models, single-cell RNA sequencing has been utilized for unbiased transcriptional profiling. However, an organized and integrated human single-cell RNA-sequencing dataset, serving as a universal reference for benchmarking human embryo models, remains unavailable. Here we developed such a reference through the integration of six published human datasets covering development from the zygote to the gastrula. Lineage annotations are contrasted and validated with available human and nonhuman primate datasets. Using stabilized Uniform Manifold Approximation and Projection, we constructed an early embryogenesis prediction tool, where query datasets can be projected on the reference and annotated with predicted cell identities. Using this reference tool, we examined published human embryo models, highlighting the risk of misannotation when relevant references are not utilized for benchmarking and authentication.

Studies of early human development are of fundamental importance to promote understanding of how we are built and how human life begins. Such studies can also shed light on reasons of infertility, early miscarriages and congenital disease. Early human embryos have become more accessible as a result of increased reproductive treatments including in vitro fertilization and preimplantation genetic diagnosis[1]. However, studies of human development are still limited by the scarcity of available human embryos that are donated for research and technical and ethical/legal challenges, such as the 14 day rule, associated with studies of human embryos[2]. For these reasons, the use of stem cell-based embryo models mimicking different aspects of human embryogenesis from the zygote stage to gastrulation has the transformative potential for advancing understanding of early human development[2,3]. However, to establish the usefulness of these models, it is critical to validate and benchmark them against human embryos of corresponding developmental stages to ensure their resemblance and fidelity to the in vivo human embryos they aim to model. Such comparison and validation should be conducted at molecular, cellular, morphological and, when possible, functional levels[4,5]. Molecular characterizations of human embryo models are commonly conducted by examining expression levels of individual lineage markers. However, it is increasingly recognized that cell types and their states are not always distinguishable with individual or a limited number of lineage markers, as many cell lineages that codevelop in early human development share the same molecular markers. As such, global gene expression profiling becomes necessary and offers an opportunity for unbiased transcriptome comparison between human embryos models and their in vitro counterparts. Although still limited, there are a few human embryo transcriptome datasets that have been reported during the last 10 years, covering human developmental stages from the fertilization to the gastrulation[6–11]. Efforts have been made to integrate these datasets; however, a well-organized and comprehensive human single-cell RNA-sequencing (scRNA-seq)

A full list of affiliations appears at the end of the paper. ✉e-mail: sophie.petropoulos@ki.se; fredrik.lanner@ki.se

dataset that could serve as a universal reference for benchmarking human embryo models remains unavailable[12–17]. Here, we developed such a human embryo development reference dataset through integration of the transcriptome data from six publicly available human datasets covering developmental stages from the zygote to the gastrula. Lineage annotations are contrasted and validated with corresponding available human and nonhuman primate datasets. Using this comprehensive and integrated reference dataset, we performed detailed comparisons with recently reported human embryo models, which revealed the risk of misannotation of cell lineages in embryo models when relevant human embryo references, such as the one developed in this work, were not utilized for benchmarking and authentication. To make our integrated reference dataset available for the public, we further developed a robust, user-friendly online early embryogenesis prediction tool, which can be utilized for benchmarking stem cell-based embryo models and human embryo-derived datasets. Further, we have also created two Shiny interfaces for convenient exploration of our reference datasets as well as primate comparative studies.

Results

Establish human embryo reference from zygote to gastrula

To create a human embryogenesis transcriptome reference covering these developmental stages, we collected six published datasets generated with scRNA-seq. We reprocessed these datasets, including mapping and feature counting, using the same genome reference (v.3.0.0, GRCh38) and annotation through a standardized processing pipeline (Methods). This approach was adopted to minimize potential batch effects as much as possible. These datasets include cultured human preimplantation stage embryos, three-dimensional (3D) cultured postimplantation blastocysts and a Carnegie stage (CS) 7 human gastrula at embryonic day (E) 16–19 isolated in vivo[6–11] (Fig. 1a). For integration of these datasets, we employed fast mutual nearest neighbor (fastMNN) methods[18] to establish a high-resolution transcriptomic roadmap. In total, expression profiles of 3,304 early human embryonic cells were embedded into the same two-dimensional (2D) space (Fig. 1a, Extended Data Fig. 1a and Supplementary Data 1). Considering both the published and updated cell type annotations, the resulting Uniform Manifold Approximation and Projection (UMAP) displays a continuous developmental progression with time and lineage specification and diversification (Fig. 1b,c). The first lineage branch point occurs as the inner cell mass (ICM) and trophectoderm (TE) cells diverge during E5, followed by the lineage bifurcation of ICM cells into the epiblast and hypoblast (Fig. 1c and Extended Data Fig. 2a)[6,10,19]. In the UMAP, early epiblast cells from E5 to E8 cluster together, whereas the majority of epiblast cells from E9 to CS7 form a distinct cluster annotated as 'late epiblast' (Extended Data Fig. 1a–d). A similar transition was observed from early to late hypoblast, occurring around E10 (Extended Data Fig. 1a–d). The UMAP also reveals that following extended 3D culture of human blastocysts, the TE matures into cytotrophoblast (CTB), syncytiotrophoblast (STB) and extravillous trophoblast (EVT), consistent with original annotations by Xiang et al.[7] (Fig. 1b,c and Extended Data Fig. 1a,d). Cell cluster annotation of the CS7 gastrula dataset in the UMAP also revealed further specification of the epiblast into the amnion, primitive streak (PriS), mesoderm and definitive endoderm (DE), together with extraembryonic lineages including yolk sac endoderm (YSE), extraembryonic mesoderm (ExE_Mes) and hematopoietic lineages (hemato-endothelial progenitors (HEP) and erythroblasts), in agreement with original annotations by Tyser et al.[8] (Fig. 1b,c and Extended Data Figs. 1a and 3c). The amnion has been suggested to form in two distinct waves[14]. In addition to the amnion cells in the CS7 dataset[8], an earlier wave was postulated to occur in extended culture of human blastocysts[7]. As the majority of those cells intermingle with advanced mesoderm (Adv_Mes) and ExE_Mes cells from CS7 gastrula in our atlas (Extended Data Fig. 1f), we do not annotate those as amnion in accordance with previous literature[7,20].

We then performed single-cell regulatory network inference and clustering (SCENIC) analysis[21] to explore the activities of different transcription factors based on mutual nearest neighbor (MNN)-corrected expression values of these transcription factors across different embryonic time points. This analysis captured some known transcription factors known to be important for different cell lineage development, thus confirming lineage identities and working as a complement to the similar analysis reported in Chen et al.[22], Mole et al.[12], Weatherbee et al.[13] and Fernandez-Gallardo et al.[23], which were performed only for certain cell lineages or developmental stages. For example, we observed signatures of important transcription factors such as *DUXA* in 8-cell lineages[10], *VENTX* in the epiblast[24], *OVOL2* in the TE, *TEAD3* in STB, *ISL1* in amnion[25], *E2F3* in erythroblasts and *MESP2* in mesoderm[26], while ExE_Mes is enriched in *HOXC8* signatures (Extended Data Fig. 1e).

Slingshot trajectory inference[27] based on the 2D UMAP embeddings revealed three main trajectories related to the epiblast, hypoblast and TE lineage development starting from the zygote (Extended Data Fig. 2a). In the epiblast, hypoblast and TE trajectories, 367, 326 and 254 transcription factor genes, respectively, were identified to show modulated expression with inferred pseudotime (Extended Data Fig. 2b and Supplementary Data 2). Transcription factors such as *DUXA* and *FOXR1* exhibit high expression during morula stages but decrease their expression during the development of all three lineages (Extended Data Fig. 2b,d). For the epiblast developmental trajectory, pluripotency markers such as *NANOG* and *POU5F1* are expressed in the preimplantation epiblast and decrease their expression following implantation, whereas *HMGN3* shows upregulated expression at the postimplantation stages (Extended Data Fig. 2b–d). Along the hypoblast trajectory, *GATA4* and *SOX17* show early expression while *FOXA2* and *HMGN3* demonstrated increased expression in the later stages. Within the TE trajectory, *CDX2* and *NR2F2* show early expression while *GATA2*, *GATA3* and *PPARG* show increased expression during TE development to CTB (Extended Data Fig. 2b,d). Notably, *HMGN3* is also associated with the later stage of the TE trajectory in a similar manner as seen in the epiblast and hypoblast trajectories (Extended Data Fig. 2b and Supplementary Data 2), a pattern also observed in the nonhuman primate transcriptome datasets[25,28–31]. Comparing the epiblast with the TE trajectories, genes such as *ZSCAN10* and *NR2F2* are specifically associated with the epiblast and TE trajectories, respectively, as they segregate from each other. Comparing the epiblast with the hypoblast trajectories, genes such as *GATA4* are specifically associated with the hypoblast trajectory (Extended Data Fig. 2b,c and Supplementary Data 2). Together, these trajectory inference analyses provide useful information for further functional characterization of key transcription factors that may play roles in driving the differentiation of the three main lineages in early human development (Supplementary Data 2).

We next identified unique markers for each distinct cell cluster from the zygote to the gastrula, including the known expression of *DUXA* in morula[32,33], *PRSS3* in ICM cells[19], *TDGF1* and *POU5F1* in epiblast, *TBXT* in PriS cells, *ISL1* and *GABRP* in amnion[25,34] and *LUM* and *POSTN* in ExE_Mes[35] (Fig. 1d and Supplementary Data 3). In addition, we identified genes such as *RBP4* (ref. 36) and *AFP*[37] that were specifically upregulated in YSE but not in the hypoblast or DE (Supplementary Fig. 1a). When comparing ExE_Mes with embryonic mesoderm, genes including *DCN*, *ANXA1* and *POSTN* are specifically expressed in ExE_Mes but not in embryonic mesoderm[35]. In contrast, *ZNF738*, *TUBB2B* and *NPY* are enriched in embryonic mesoderm compared with ExE_Mes (Supplementary Fig. 1b). Further examination of the four subpopulations of HEP based on the reference UMAP shows that hemogenic endothelium stretches from the ExE_Mes to the HEP clusters (Supplementary Fig. 1c).

Given the enrichment of key marker genes and transcription factor regulatory networks, we are confident that our embryonic reference provides reliable transcriptome profiles for each lineage present in early human embryo development included in those datasets.

https://doi.org/10.1038/s41592-024-02493-2

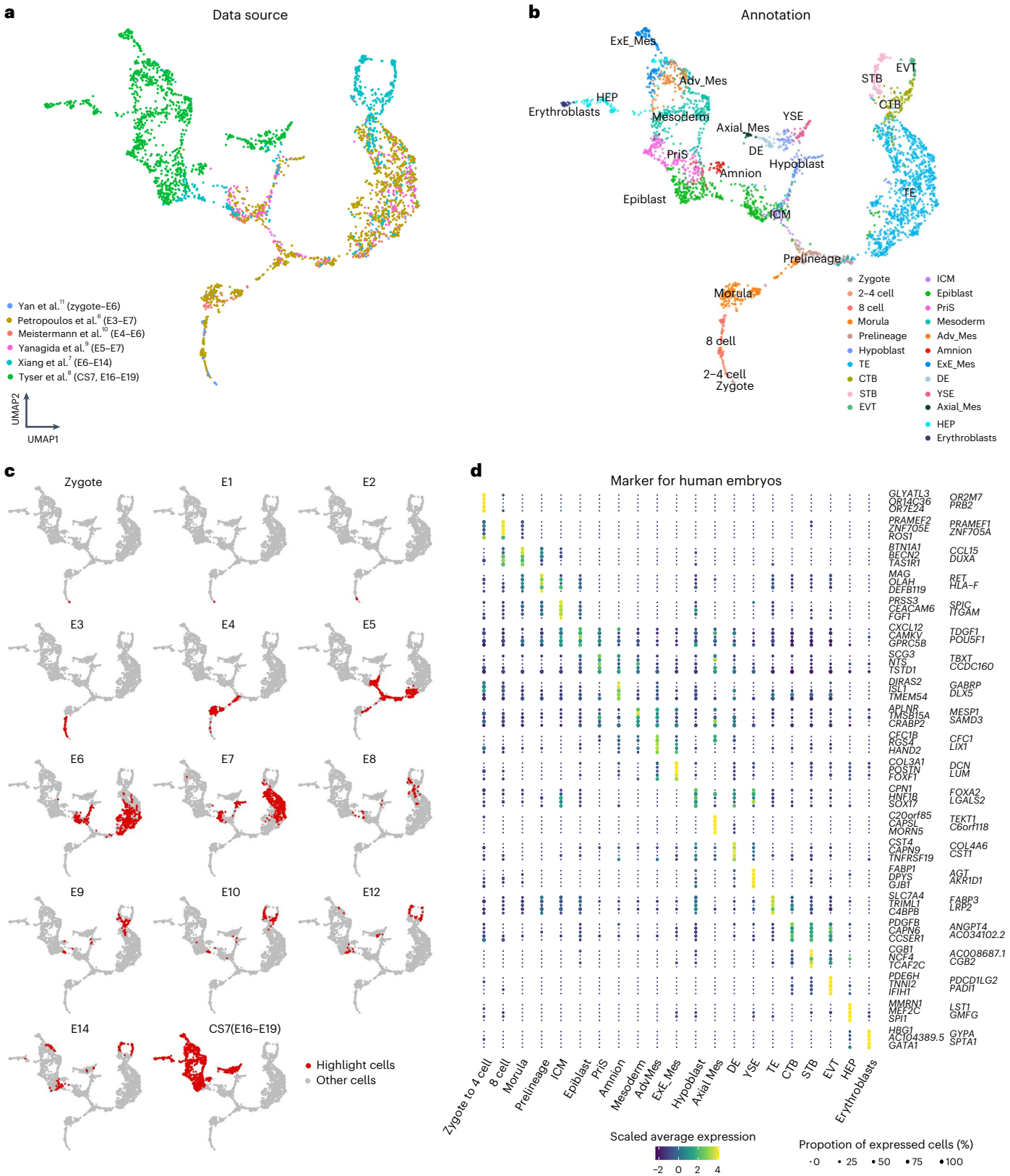

Fig. 1 | Construction of a human embryonic reference from zygote to the gastrula. a, A UMAP projection of the integration of six embryonic datasets. The color of each data point represents the source of the data. **b**, Similar to **a**, but the color indicates the cell annotations retrieved from each publication. **c**, Cells from different embryonic time points are highlighted on the human embryonic reference. **d**, A dot plot illustrating the expression of the top five lineage-specific genes used in the human embryonic reference. The size and colors of dots indicate the proportion of cells expressing the corresponding genes and scaled values of log-transformed expression, respectively.

Integration with nonhuman primates

It should be acknowledged that the existing human embryo reference datasets are still limited, with data from one single in vivo gastrulating embryo[8]. We therefore compared the six human embryo datasets with additional datasets from cynomolgus macaque, encompassing transcriptome profiles for preimplantation embryos[29], embryos collected during gastrulation[30] and in vitro cultured postimplantation embryos[25]. Furthermore, two additional datasets from the marmoset were also included, comprising a transcriptome profile for preimplantation embryos[28] and implanted marmoset embryos at CS5–7, including spatial information[31]. Considering the effective performance of the MNN method in removing batch effects among datasets, similar MNN expression correction was performed for datasets from each species to eliminate intraspecies batch differences. This was followed by canonical correlation analysis to simultaneously anchor all datasets[38]. Through these efforts, single-cell transcriptional profiles from 11 datasets across three primate species were successfully embedded into the same 2D UMAP space (Extended Data Fig. 3a,b). This integrated UMAP revealed a continuum of transcriptome state changes. Cell lineage annotations and associated developmental stages reported identified in the UMAP also matched those by the original publications (Extended Data Fig. 3a and Supplementary Fig. 2), thus confirming that intra/interspecies batch differences were effectively removed during the aforementioned process.

From the cross-species integration, we observed that lineage developments from the prelineage to ICM and TE, from the ICM to epiblast and hypoblast, from the epiblast to PriS, mesoderm and amnion, and from the TE to CTB, STB and EVT, were well conserved in all primate species (Extended Data Fig. 3a,c). Marmoset embryonic disc (EmDisc) cells overlap with late epiblast-related lineages of the CS7 human gastrula, including the 'epiblast', 'PriS', 'mesoderm' and E16–E17 epiblast cells in cynomolgus monkey (Extended Data Fig. 3a,c and Supplementary Fig. 2). Visceral endoderm (VE) and YSE populations overlap well between human and marmoset datasets (Extended Data Fig. 3a,c). Marmoset cells reported with uncertain identity in the original report among CS7 secondary yolk sac, ExE_Mes, matched with secondary yolk sac and amnion cells in our analysis[31]. 'Gastrula' (Gast) cells in cynomolgus monkey overlapped with corresponding cell clusters in the human gastrula, including the mesoderm and PriS cells. Some cells identified as 'Gast' cells mainly from E16 and E17 cynomolgus monkey are aligned to part of the human Adv_Mes (Extended Data Fig. 2a,c and Supplementary Fig. 2). The position of cells from 'Amnion_Gast' from cynomolgus monkey[30] overlap with cells from the human dataset, validating their identity as true amnion cells[8]. In addition, we observed that extraembryonic cells (ExE_Mes cells, stalk and extraembryonic mesenchyme) formed large clusters. Human Adv_Mes cells were situated between and intermixed with the embryonic mesoderm cells and extraembryonic cells on the reference map as a result of transcriptional similarities. On the basis of this observation and further analysis, we annotated 53 Adv_Mes cells as ExE_Mes ('Restoration of previous annotations for published datasets' section).

Utilizing the comprehensive primate reference, we identified conserved markers for the major lineages, including well-known pluripotency markers such as *SOX2* and *NANOG* for the epiblast, *SOX17* and *FOXA2* for endoderm cells, *GATA2* and *GATA3* for TE and its derivatives, *DCN* and *VIM* for extraembryonic cells and *GABRP* and *ISL1* for amnion cells (Extended Data Fig. 3d and Supplementary Data 4). Interestingly, some genes, such as the protein-coding gene *FAM124A*, whose function is uncertain, *MUSTN1*, which is related to the musculoskeletal system and normal embryo development[39], *LIM2*, which encodes an eye lens-specific protein and *ADAM15*, which is involved in cell adhesion[40], were identified as specific to human lineages but not to other nonhuman primates (Supplementary Fig. 3 and Supplementary Data 4). Thus, this comprehensive integrated scRNA-seq dataset of early primate embryos provides a framework for investigating the concordance and variance among different species. Importantly, nonhuman primate datasets provide further support to the annotations in our human embryogenesis reference.

Stabilized query projection onto human embryonic reference

Having characterized the assembled human embryo reference dataset, we next sought to use this to establish a stabilized UMAP for evaluating the validity of stem cell-based embryo models. To achieve this, we distilled the entire fastMNN reference construction process into three major parts: (1) rescaling normalization, (2) principal component analysis (PCA) subspace projection after MNN correction and (3) UMAP projection (Fig. 2a). Throughout this analysis, adhering carefully to the assumptions that MNN pairs define the most similar cells of the same type across batches[18], we divided the query data into small samples and filtered ambiguous pairs (Extended Data Fig. 4a,b and Methods). After generating comparable normalized data for the query dataset, it was projected onto the same PCA subspace and subsequently corrected in accordance with Haghverdi et al.[18], followed by projection onto the same UMAP space as the reference (Fig. 2a). In addition, we trained support vector machine (SVM) classifier models for each lineage of reference cells in a 20-dimensional latent space, optimizing the hyperparameters for each model. Once the query cells were successfully transformed into the same latent space as the reference, their identities were predicted using these pretrained reference SVM models (Fig. 2a and Extended Data Fig. 4c). Query cells that did not correspond to those in our reference were filtered out based on correlation filtering and annotated as 'nonrelated' (Extended Data Fig. 4f and Methods).

To test the prediction performance and determine the best parameters for our prediction tool, entitled the early embryogenesis prediction tool, five additional embryonic datasets were utilized, including a prelineage embryo dataset spanning from the 2-cell to morula stage[41], a blastocyst dataset[42] and three peri-implantation and postimplantation datasets[12,43,44] (Fig. 2b,c). Of note, regardless of the library preparation utilized to generate these datasets (for example, Smart-Seq2, Trio-seq

Fig. 2 | Validation of the early embryogenesis prediction tool. a, The processing workflow to project query cells onto the reference and cell type prediction. (1) Query data underwent rescaled normalization to ensure that expression values were comparable with the reference datasets. This step was taken after deciding whether to aggregate cells into neighborhoods for low-depth, large datasets. Cosine normalization of query expression involved removing the same grand center values from reference calculations and performing a dot product calculation with the left singular vectors (U) obtained from singular value decomposition during reference construction. (2) Orthogonalization removes variation along the reference batch correction vector, projecting onto the reference PCA subspace. Simultaneously, the query dataset was divided into smaller samples consisting of 200 cells, repeated five times, to calculate MNN pairs with the reference datasets separately. Uncertain MNN pairs were removed. Using the filtered MNN pairs, a batch correction vector was computed to correct the PCA coordination of the query dataset. (3) UMAP embedding was transformed using the UMAP model calculated from the reference (ref) dataset. Cell identities were predicted using the SVM models trained on the reference datasets within the same latent space after UMAP transformation. TE, trophectoderm; Am, amnion; r, repeat times. **b**, Projection of five embryonic datasets onto the human embryonic reference. The color represents the cell annotations for each publication. The light-gray points represent cells used in embryonic reference construction. **c**, An alluvial plot comparing the original cell type to the predicted identities from the early embryogenesis prediction tool. Predictions identified as 'ambiguous' or 'nb_failed' represent cells with uncertain predictions or cells that fail to form neighborhoods, respectively. **d**, Prediction precision and recall ratio for each cell type in the embryonic datasets. The shape and color indicate queried cell types and data sources, respectively. ysTE, yolk sac TE; VE/YE, visceral/yolk endoderm; AVE, anterior VE.

https://doi.org/10.1038/s41592-024-02493-2

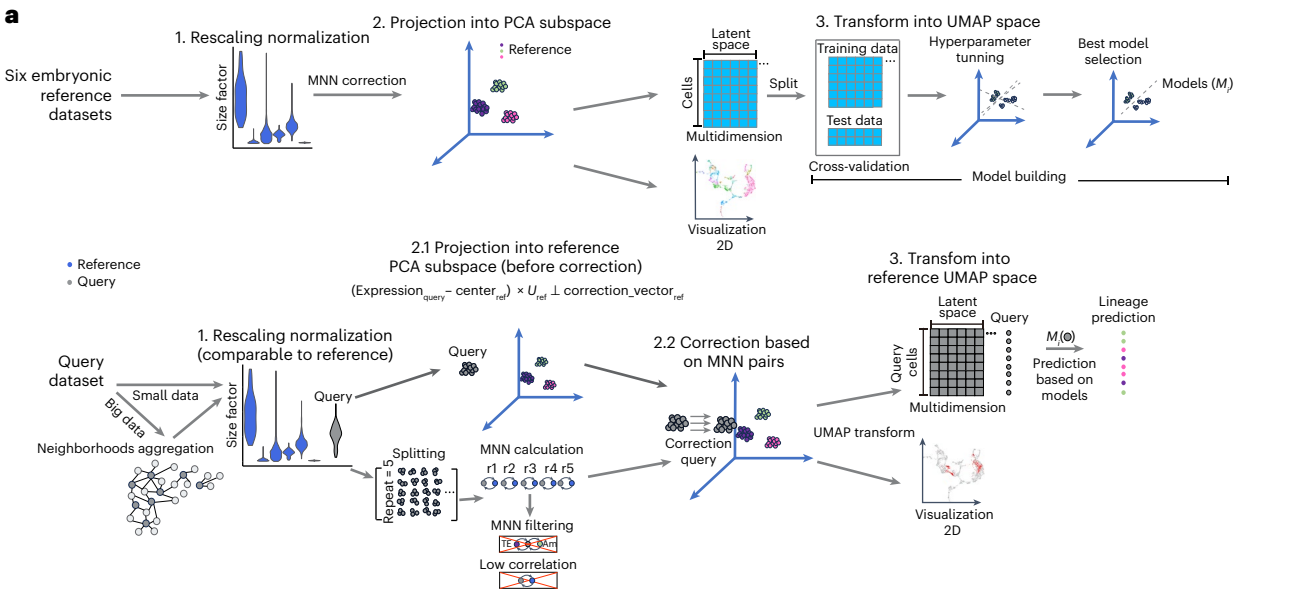

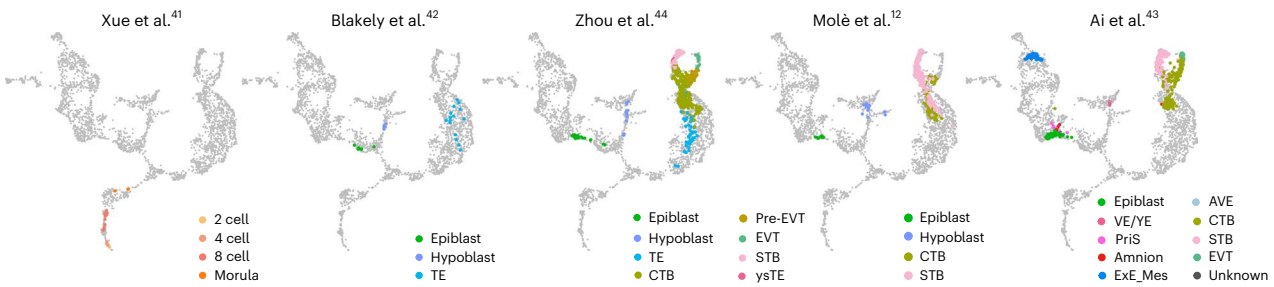

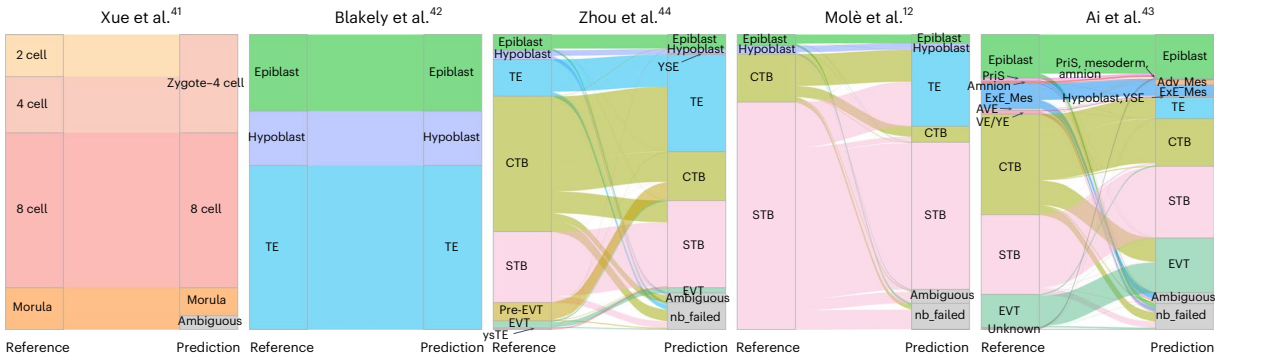

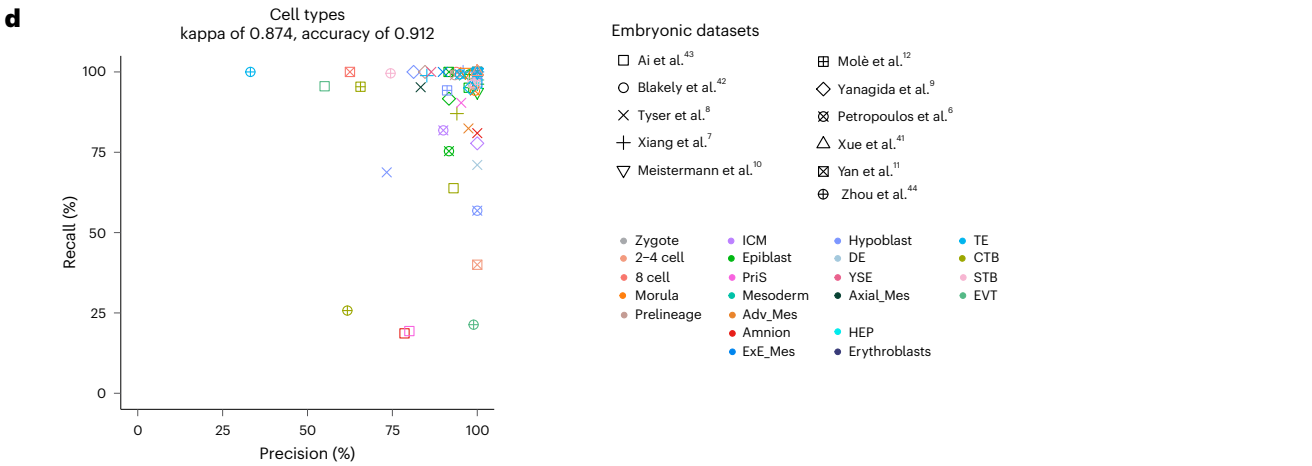

or 10x sequencing) or whether the datasets were used as processed by the authors or reprocessed in-house, cell clusters in all five datasets displayed good alignments with their counterparts in our human embryo development reference dataset (Fig. 2b,c and Supplementary Fig. 4). Overall, we achieved a 0.961 kappa value and 0.982 accuracy when comparing published annotations of the main lineages during human embryo development with our predictions (Extended Data Fig. 4e). When considering a more granular classification of sublineages, we obtained a 0.874 kappa value and 0.912 accuracy (Fig. 2d). In addition, our prediction tool performed better than current methods such as SingleR[45], scMap[46] and scType[47] in classification metrics, including kappa score and accuracy (Extended Data Fig. 4d). Our tool demonstrated robust prediction power for all lineages across all embryonic datasets (Fig. 2d and Extended Data Fig. 4d). Thus we conclude that this predictive pipeline delivers a highly accurate performance for scRNA-seq datasets, irrespective of upstream library preparation or data processing, which can be leveraged for benchmarking stem cell-derived embryo models and newly generated embryonic datasets.

Mapping stem cells and derived lineages

Naive and primed human pluripotent stem (hPS) cells are considered analogous to the embryonic epiblast at preimplantation and perigastrulation stages, respectively. As expected, naive hPS cells were mapped to early epiblast cells before E9, whereas primed cells were projected to late epiblast cells (Figs. 1c and 3a and Extended Data Fig. 1c). Trophoblast stem cells, derived from blastoids using Okae et al. culture conditions[48,49], mapped to E7–E10 TE and CTB cells, confirming their trophoblast identity. There is a longstanding debate whether human naive and primed hPS cells can be converted to trophoblast lineages[5,50,51]. One concern has been that converted putative trophoblast cells instead may be misannotated ExE_Mes or amnion lineage as some lineage markers are shared between these lineages[52,53]. For these reasons, we assessed the transcriptional profiles of published TE-like cells (TLCs) derived from naive and primed hPS cells, in addition to our own unpublished dataset of primed hPS cell-derived TLC (in-house) (Fig. 3b)[50,54–57]. Both naive and primed hPS cell-derived TLC were predicted as TE cells of the blastocyst or later trophoblast lineages. However, primed hPS cell-derived TLC also contained notable populations of both amnion and ExE_Mes cells (Fig. 3c). These predictions were confirmed by module score calculation based on lineage marker genes (Extended Data Fig. 5a,b).

It has been suggested that human trophoblast stem cells are more similar to postimplantation trophoblast lineage or even first-trimester placental cells[22,58,59]. Since our reference atlas does not include such later stage cells, we decided to include two additional datasets to our existing atlas (Methods). One dataset is from recently published spatial transcriptomics of a CS8 human embryo[60] and the other comprises 10x-sequenced single-cell transcriptomes of STB, EVT and villous CTB from first-trimester placentas[61] (Extended Data Fig. 6a). According to this extended reference, CTB from first-trimester placentas clustered distinctly from CTB of peri-implantation embryos, whereas STB and EVT in first-trimester placentas and peri-implantation embryos were more closely related (Extended Data Fig. 6a). Using the same projection strategy as above, we projected the six datasets of human trophoblast stem cells derived from naive and primed hPS cells and an additional dataset from organoids derived from the first-trimester placenta[59] onto this extended reference. TLCs derived from naive and primed hPS cells projected to pre- and peri-implantation TE lineage cells. In contrast, organoid cells derived from the first-trimester placenta projected more closely to first-trimester placenta cells (Extended Data Fig. 6b). Therefore, we conclude that TLCs derived from naive and primed hPS cells are more similar to pre- and peri-implantation TE lineages rather than to first-trimester placenta cells.

Among the 705 differentially expressed genes (DEGs) between naive and primed hPS cells, 32, 47 and 51 were also differentially expressed in the amnion, ExE_Mes and PriS, respectively, when compared with preimplantation TE cells (Supplementary Fig. 5 and Supplementary Data 5). Interestingly, DEGs highly expressed in amnion, ExE_Mes and PriS were also expressed specifically in the primed hPS cells (18 out of 18 genes). Conversely, genes preferentially expressed in TE cells were also enriched in naive hPS cells (49 out of 56 genes) (Supplementary Fig. 5d–g and Supplementary Data 5). The genes shared by naive hPS cells and TE cells, including transcriptional factors *NLRP2*, *NLRP7*, *TFAP2C*, *KLF4* and *ELF3*, may facilitate naive hPS cells to adopt a TE fate over alternative fates including amnion, ExE_Mes and PriS (Supplementary Data 5). We next compared the TLCs generated from both naive and primed hPS cells with the preimplantation TEs. We identified 129 and 196 DEGs consistently differentially expressed in naive or primed hPS cell-derived TLCs when compared with TE cells (Fig. 3d and Supplementary Data 6). Seventy-eight of these DEGs were shared in both naive and primed hPS cell-derived TLCs (Fig. 3e and Supplementary Data 6). TE transcription factors such *CDX2* and *GTSF1* were expressed at low levels in primed hPS cell-derived cells, while *HES4* (hes family bHLH transcription factor 4), which participates in transcriptional regulation and the Notch signaling pathway, was expressed only in stem cell-derived TLCs (Supplementary Fig. 6). *DNMT3L* involved in the process of DNA methylation was expressed at low levels in both naive and primed hPS cell-derived TLCs, and was particularly low in primed hPS cell-derived TLCs (Supplementary Fig. 6). *XIST* levels were also absent in primed hPS cell-derived TLCs, while some naive hPS cell-derived TLCs expressed significant levels of *XIST* (Fig. 3e and Supplementary Fig. 6), which suggests that primed hPS cell-derived TLCs might have an aberrant epigenetic state.

We next applied our reference map to evaluate published studies of differentiating naive and primed hPS cells into ExE_Mes and amnion, respectively[17,35], and confirmed the accurate annotations of naive hPS cell-derived ExE_Mes cells as well as primed hPS cell-derived amnion in the stem cell-based, postimplantation amniotic sac embryoid (PASE) model (Fig. 3f,g). The PASE model also includes PriS- and mesoderm-like cells, which map as expected onto their in vivo counterparts of our reference map, while the primordial germ cell (PGC)-like cells developed in the PASE overlap with the PriS cells in our reference map. This observation suggests that our current reference can not readily resolve PGCs, as the original human gastrula dataset only included seven annotated PGCs, which is not enough to establish a discrete cluster on our reference UMAP.

There are recent studies reporting transient conversion of hPS cells into 8-cell-like cells (8CLC). Indeed, we observed a large proportion of

Fig. 3 | Application of the early embryogenesis prediction tool on stem cell models. a, The projection of naive, primed and Okae cells from Kagawa et al.[48] onto the reference. The color of each data point represent the cell identity and gray cells the reference. **b**, The projection of naive or primed hPS cell-derived TLCs. **c**, A bar plot showing the proportion of predicted cell identities for naive and primed hPS cell-derived cells. **d**, A Venn diagram showing the overlap of DEGs between naive or primed-derived preimplantation TLCs and embryonic preimplantation TE cells. **e**, A heat map showing the expression of DEGs in preimplantation TLCs and embryonic preimplantation TE cells. The DEGs were conserved in all three naive hPS cell-derived TLC comparisons or conserved in all three primed hPS cell-derived TLC comparisons, primed hPS cell-derived TLCs and embryonic TE cells. **f**,**g**, The projection of cells (neighborhood nodes) from two studies modeling ExE_Mes cells and PASE. A bar plot showing the proportion of predicted cell identities stratified by cell types or time point. **h**,**i**, The projection of cells (neighborhood nodes) from two studies modeling 8CLCs. A bar plot showing the proportion of predicted cell identities stratified by cell original annotation. EPI, epiblast; PE, primitive endoderm; TSC, trophoblast stem cells; ExE_MeLC, extraembryonic mesoderm-like cell; PGC_like, PGC-like cell; MeLC, mesoderm-like cell; AMLC, amnion-like cells; 4CL, 4 chemicals + leukemia inhibitory factor (LIF) medium; e4CL, enhanced 4CL medium; DOX, doxycycline.

https://doi.org/10.1038/s41592-024-02493-2

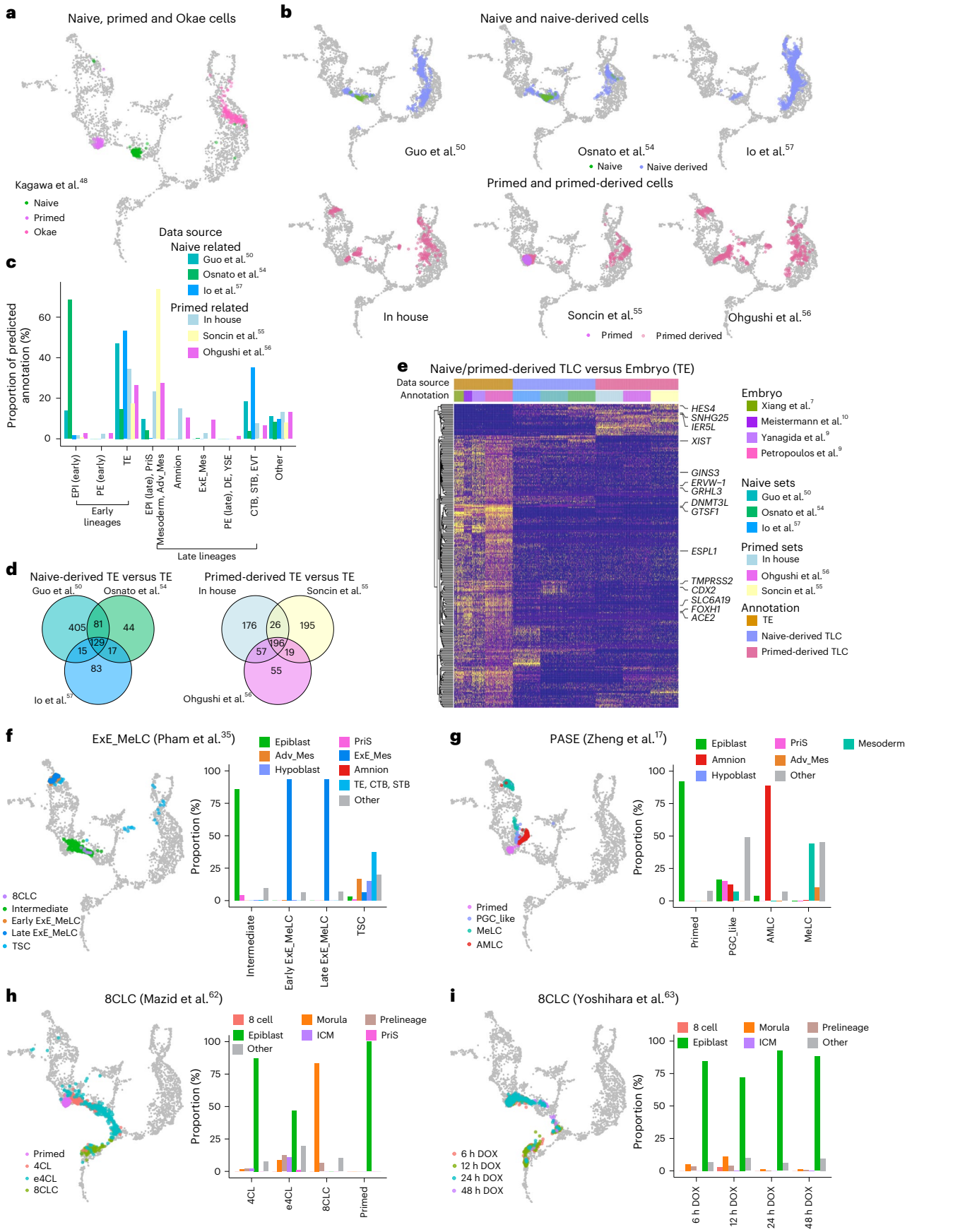

morula-like cells but not 8CLC in Mazid et al.[62], confirmed by module score calculation (Fig. 3h and Extended Data Fig. 5c). In ref. 63, we observed around 3.1% 8CLC 12 h after transient doxycycline treatment in doxycycline-inducible DUX4-TetOn hES cells, which is consistent with the data reported in the study (Fig. 3i).

Evaluating the preimplantation blastoids models

Next we explored the transcriptional profiles of blastoids established from naive hPS cells or extended pluripotent stem cells (EPS cells) or through partial reprogramming[9,16,48,64–67]. Projection of three naive hPS cell-derived blastoids reveals the presence of expected cell types, with the majority of annotated epiblast-like cells (ELC), hypoblast-like cells (HLC) and TLC overlapping with their counterparts in the human blastocyst, although a fraction of cells showed signatures more in line with postimplantation cell lineages (Fig. 4a,b and Extended Data Fig. 7). In addition, small fractions of cells with signatures resembling ExE_Mes and amnion were also detected in these naive hPS cell-derived blastoids (Fig. 4a). In blastoids generated from reprogramming of somatic human cells[65], the majority of TLCs overlap with the amnion reference (Fig. 4b). Blastoids derived from EPS cells by Sozen et al.[67] were reported to show blastocyst-like morphology but lack correct transcriptional profiles. In agreement with that finding, most cells in EPS cell-derived blastoids were predicted as ExE_Mes or Adv_Mes. EPS cell-derived blastoids from Fan et al.[66] did contain TLCs, but the majority of the cells in the blastoids resembled 'late epiblast' cells (after E9) with very few HLCs (Fig. 4b). To validate these discrepancies in cell lineage composition in an independent manner, we further utilized published cynomolgus data[25], which includes both amnion and trophoblast cells within the same dataset. Comparative transcriptome analysis of blastoids using cynomolgus data as a reference clearly shows that the majority of TLCs in blastoids of Liu et al.[65] cluster with the amnion rather than the TE lineage (Extended Data Fig. 7). The majority of TLCs in blastoids from Sozen et al.[67] are closely related to ExE_Mech (Extended Data Fig. 7). HLCs in the blastoids from Fan et al.[66] did not align with the reference endoderm cells. Additionally, TLCs in blastoids from Liu et al. lack or express low levels of TE markers such as *GATA2*, *GCM1* and *BIN2*, but instead express amnion markers *ISL1*, *GABRP* and *IGFBP7* (Extended Data Fig. 8c,d). Furthermore, we utilized DEGs between early and late stages of the epiblast and hypoblast cells (Extended Data Fig. 1d and Supplementary Data 7) and checked their expression in blastoids (Extended Data Fig. 8a,b). The ELCs in EPS cell-derived blastoids[66,67] preferentially express late epiblast DEGs but low expression levels of early epiblast DEGs, similar to primed hPS cells (Extended Data Fig. 8a). HLC of blastoids generated through partial reprogramming[65] or using EPS cells[66,67] expressed DEGs enriched in late hypoblast cells. Predicted annotations were further justified by module score calculation (Extended Data Fig. 9). Together, our analysis supports that naive hPS cell-derived blastoids are composed of cells with transcriptional profiles in line with those in human blastocysts. However, detailed analysis could still identify differences in gene expression between these naive hPS cell-derived blastoids and the human reference. On the basis of the Gene Set Enrichment Analysis (GSEA)[68] for each comparison within each lineage, pathways related to energy production, including 'oxidative phosphorylation' and 'electron transport chain oxphos system in mitochondria', were upregulated in Kagawa et al.[48] and Yu et al.[64] but not in Yanagida et al.[9] Metabolic rewiring has been suggested to be important for blastoid formation[69]. Genes related to 'focal adhesion' and the 'focal adhesion PI3K/AKT/mTOR signaling pathway', which are important for cell attachment and migration, were instead only upregulated in Yanagida et al.[9] (Fig. 4d and Supplementary Data 8). Additionally, there were 7, 9 and 48 DEGs shared by all three naive hPS cell-derived blastoids when compared with the human reference (Fig. 4c and Supplementary Data 8). Specifically, in naive hPS cell-derived blastoids, *NAA11* showed reduced expression in ELC and HLC. *OTX and HAVCR1* were also poorly expressed in ELC and HLC, respectively. Expression of *ACE2*, *FMR1NB*, *SLC6A19*, *PHOSPHO1*, *TKTL1* and *MAGEA4* were also lacking in TLC of naive hPS cell-derived blastoids (Fig. 4e). It is unknown whether these DEGs translate into functional differences but such aberrant expressions should be taken into consideration when using these models. One recent example is modeling of severe acute respiratory syndrome coronavirus 2 (SARS-CoV-2) placenta infection using stem cell models. SARS-CoV-2 infects cells via its spike protein binding to the host entry receptor angiotensin-converting enzyme 2 (*ACE2*). Several studies have examined SARS-CoV-2 infection and *ACE2* expression in trophoblast organoids and in alignment with our analysis of blastoids, they also have seen reduction of *ACE2* levels and SARS-CoV-2 infection in such in vitro models, highlighting important functional differences between stem cell models and embryonic cells[70,71].

Evaluating stem cell-derived postimplantation embryo models

Following implantation, the human embryo undergoes major organizational changes crucial for gastrulation and subsequent development. Several stem cell-derived, postimplantation models have been developed to mimic the development of human embryos during this window. In addition to capturing morphogenesis and structural similarities to human postimplantation embryos, it is important to understand which lineages they are composed of. To address this, we projected recent studies[13,43,71–75] onto our human embryogenesis reference to evaluate their similarities with postimplantation lineages (Fig. 5 and Extended Data Figs. 10a,b). Three studies[43,72,73] combine pluripotent cells with hypoblast-induced cells, generating cells with signatures aligning with the embryogenesis reference cells including epiblast, PriS, mesoderm, ExE_Mes, amnion and late hypoblast (Fig. 5). Two other studies[13,74] also included TLC in the assembloids, cultured in suspension, while the third started from naive-derived blastoids that were allowed to grow attached in 2D or imbedded in 3D[71]. The blastoid-based model had the best contribution to the TE compartment in the embryonic reference (Fig. 5 and Extended Data Fig. 10c), possibly due to the attachment strategy that might better support TE expansion. It is important to note that postimplantation models do not necessarily need to capture all lineages of the human embryo to be useful. This is exemplified in the recent study by Hislop et al.[75], which modeled postimplantation development without a TE compartment but succeeded in establishing yolk sac hematopoiesis, which was evident also from mapping to the embryogenesis reference (Fig. 5). Further, our tool was unable to resolve amnion cells from Pedroza et al.[72] and Karvas et al.[76], possibly due to two distinct reasons. We observed that amnion-annotated cells from Pedroza et al.[72] are projected together with epiblast and PriS. Using the published annotations and gene expression matrix from Pedroza et al.[72],

Fig. 4 | Application of early embryogenesis prediction tools on preimplantation blastoid models. a,**b**, The projection of blastoid cells (or neighborhood nodes) onto the human embryonic reference in naive-derived blastoids (**a**) and reprogrammed or EPS cell-derived blastoids (**b**). The color of each data point represents the cell annotations retrieved or restored for each publication. Light gray data points indicate cells used in embryonic reference construction. An alluvial plot comparing original cell-type annotations (ELC, HLC and TLC from the six blastoids) to the predicted identities obtained from the early embryogenesis prediction tool. **c**, A Venn diagram showing the overlaps of DEGs between blastoids with preimplantation embryonic lineages for three naive-derived blastoids. **d**, Selected significant Wikipathways demonstrating differences among the three naive-derived blastoids (Bla1–3) and preimplantation embryos from the embryonic reference, stratified by lineage. The colors indicate the normalized enrichment score (NES) and the size represents the Benjamini–Hochberg-adjusted *P* values from one-sided tests. **e**, Violin plots showing the expression of representative DEGs between blastoids (Bla1–3) and embryonic references (EM1–4). low_cor, low-correlation filtered.

https://doi.org/10.1038/s41592-024-02493-2

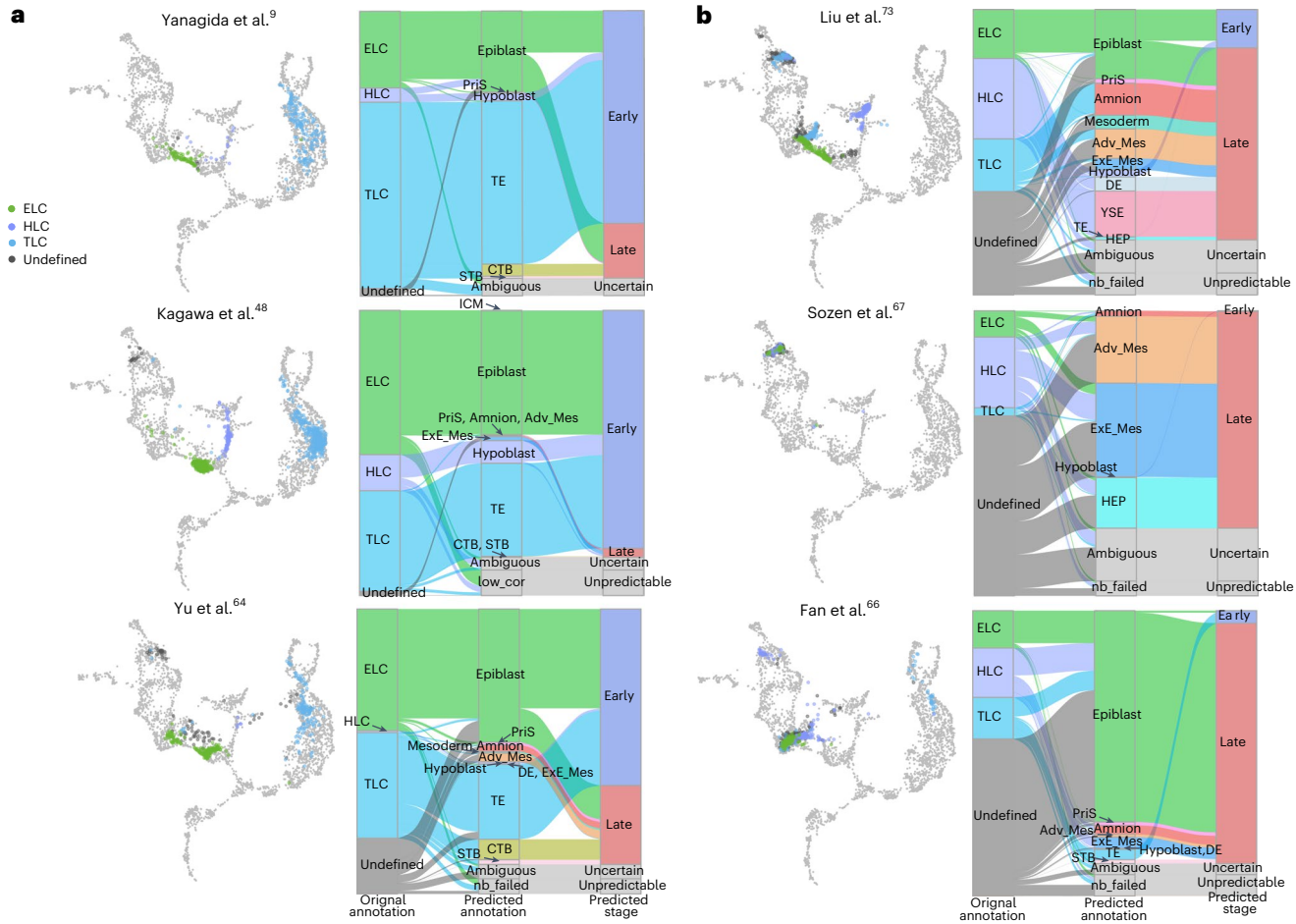

https://doi.org/10.1038/s41592-024-02493-2

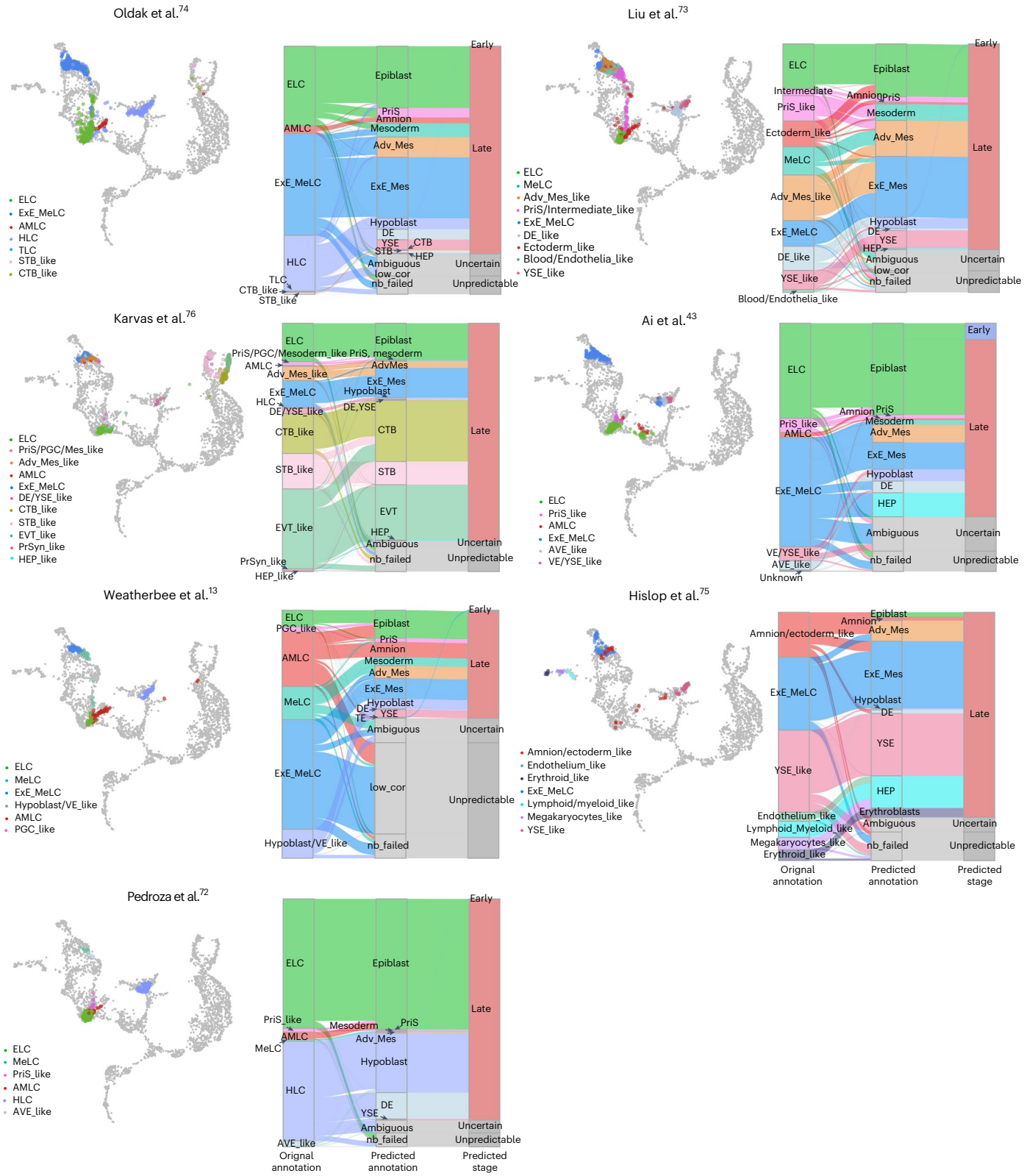

Fig. 5 | Application of early embryogenesis prediction tools on postimplantation blastoid models. The projection of blastoid cells (or neighborhood nodes) onto the human embryonic reference (left side of each reference image). The color of each data point represents the cell annotations retrieved or restored for each publication. The light gray data points indicate cells used in embryonic reference construction (right side of each reference image). The alluvial plots compare original cell-type annotations to the predicted identities obtained from the early embryogenesis prediction tool. ExE_MeLC, extraembryonic mesoderm-like cell; PGC_like, PGC-like cell; MeLC, mesoderm-like cell; AMLC, amnion-like cells; STB_like, STB-like cells; CTB_like, CTB-like cells; YSE_like, YSE-like cell; EVT, EVT-like cell; HEP_like, HEP-like cell; PriS_like, PriS-like cell; AVE_like, anterior VE-like cell; VE, VE-like cell; PrSyn_like, primitive syncytium-like cell; DE_like, definitive endoderm-like cells; AdvMes_like, advanced mesoderm-like cells; Blood/Endothelia_like, blood/endothelia-like cells; PriS/Intermediate like, primitive streak/intermediate-like cells; Ectoderm_like, ectoderm-like cells.

https://doi.org/10.1038/s41592-024-02493-2

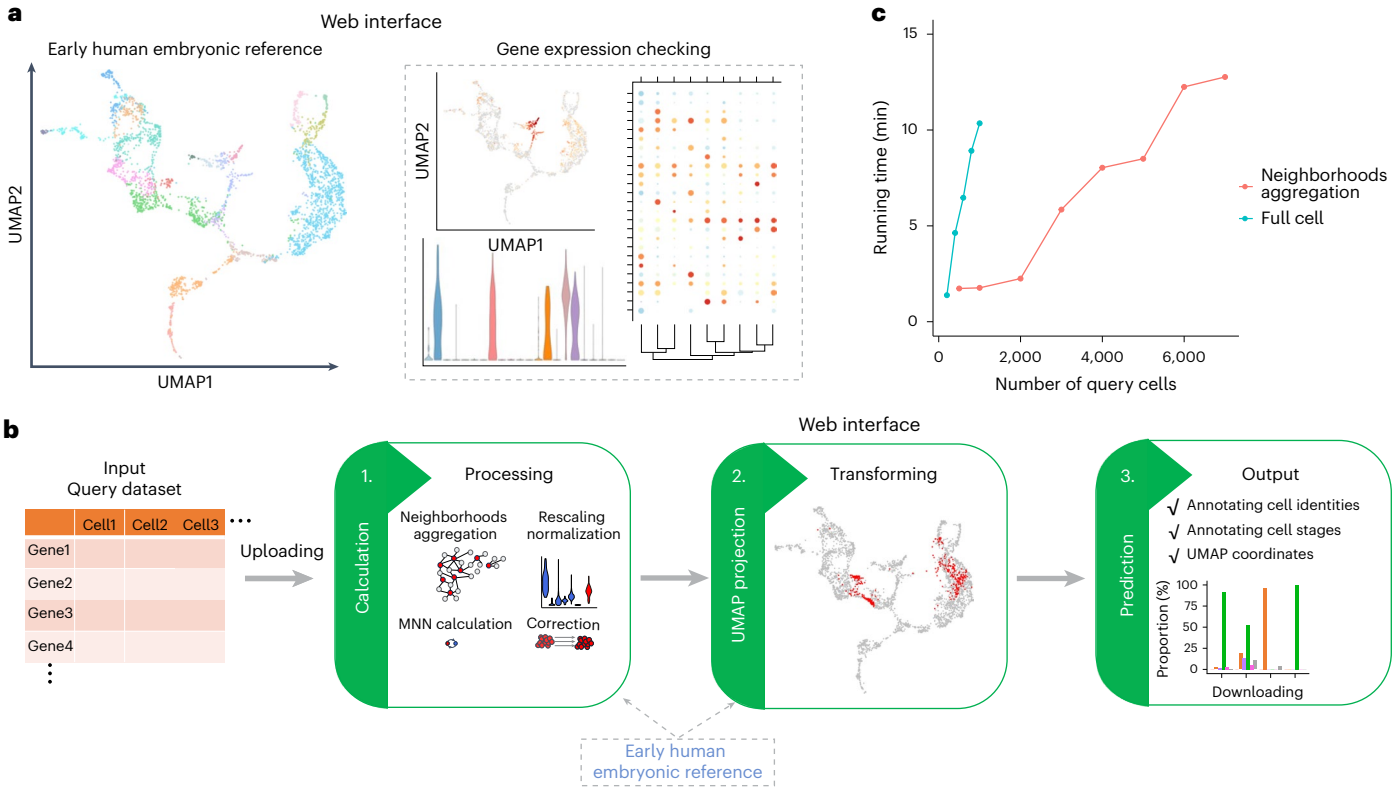

Fig. 6 | Web interface for our online resources. a, A schematic of the web interface for the human embryonic reference. **b**, A schematic of the web interface for the early embryogenesis prediction tool. **c**, The running time for webtool with different numbers of query cells.

we identified that only 62 out of 460 amnion-annotated cells exhibited at least one read for any one of the amnion markers, *ISL1*, *GABRP*, *VIT*, *VTCN1*, *WNT4* or *WNT6*, which is insufficient to classify as amnion. It is still possible that there are early amnion cells in this dataset, which are lacking in the Tyser et al.[8] reference. In the Karvas et al.[76] study, less than 15 amnion cells are reported, which are interspersed with Adv_Mes-like cells[71]. In this case, the amnion cells are probably too few to form an independent amnion neighborhood, but instead mix with ExE_Mes cells in our reference map due to their shared transcriptional profiles.

A web platform for embryonic study

During this study, we have curated a total of 41 processed datasets, including their raw expression data, original annotation and predicted annotation. Among these datasets, eight human embryonic datasets, six preimplantation blastoids datasets, one 8CLC dataset and one PASE dataset were reprocessed by us using the same mapping strategy (10x using Cell Ranger[77] and non-10x using STAR[78]) and genome annotation[6–11,42,43,48,63–67]. This effort has allowed us to eliminate batch differences arising from different processing pipelines or gene annotations, providing a valuable resource for future investigations.

To facilitate comparative studies and easy access to analysis of single-cell datasets related to the developmental stages of zygote to gastrulation, we have developed an interactive online tool based on the human embryogenesis reference and the extended primate cross-species embryonic reference using ShinyCell[79] (Fig. 6a). This can be used to browse the expression of selected genes in both the human and primate reference atlas. Furthermore, we have transformed the prediction pipeline into an online analytical application, which we entitled the early embryogenesis prediction tool (Fig. 6b). Our primary focus was to create a user-friendly interface, ensuring that researchers can directly access and utilize it by providing only the gene expression matrix. The entire process of normalization, projection and annotation takes less than 15 min for fewer than 7,000 cells (Fig. 6c).

We envision broad usage of these assembled datasets and online tools for the authentication of human embryo models, in turn supporting the development and application of this emerging field.

Discussion

In this Resource, we have integrated available human embryo datasets to create a transcriptional reference map of human embryonic development from zygote to gastrula. This assembled dataset will hopefully facilitate deeper understanding of the transcriptional networks that are operating and directing early human embryo development. The resource will also aid in validating and aligning stem cell-based embryo models with embryo equivalents, while also providing a transcriptional benchmark for the development of future models and optimization of stem cell cultures. The embryonic reference tool effectively distinguished early human embryo identities from different stages and lineages. We anticipate that the strategy we utilized for building the reference atlas, project and predict query datasets can be extended to other developmental stages, specific organs and other species, although this is outside the scope of the current study. The development of our reference depended on the quality of the datasets utilized and, as such, if datasets of lower quality or richness (for example, cell types lacking, insufficient number of cells, shallow read depth and so on) would be incorporated, it would result in reduced precision. That said, we have demonstrated the expandability of our embryonic reference, even when shallow sequenced datasets are utilized, though not ideal as they require additional processing by aggregation. An additional caveat we need to stress is that the incorporation spatial transcriptional analysis is not at a single-cell level, which impacts the utility of the cellular signatures as multiple cell types may be captured within the same area. In both instances, we see that the strategy used for the construction of our reference is robust. This strategy may also be helpful within the field of stem cell-based cell therapies to characterize the cellular composition of on- and off-target cell types[80].

There are important limitations of our tool that should be considered when interpreting results obtained. First, an inherited limitation of MNN correction makes it challenging to correct datasets without shared similar identities. False-positive predictions may therefore occur for cells with transcriptome signatures that are not present in our reference but share close similarities. We partially resolved this issue by including correlation filtering in our processing pipeline. To test this we used unrelated datasets, including five public scRNA-seq datasets from human pancreas, macrophages, fetal kidney development and liver tissues (Methods) and determined that a median top correlation coefficient threshold of 0.5 can eliminate unrelated cell types. However, this is still an important aspect to bear in mind. Another limitation is that the embryonic reference dataset contains few PGCs, with similarities in gene expression to PriS, and could therefore not be resolved as a distinct cluster which means that we can not identify PGCs using our tool. This could be resolved in the future with additional in vivo reference datasets, ideally sequenced using Smart-seq based platforms to ensure richness of the reference. Distinguishing between ExE_Mes cells and embryonic mesoderm cells proved challenging due to shared gene expression similarities and lack of well defined markers. Cross-referencing with the spatial information provided by the marmoset dataset allowed us to reclassify some Adv_Mes cells as ExE_Mes cells. Genes specifically expressed in ExE_Mes cells, such as *DCN*, *ANXA1* and *POSTN*[35], may be helpful in addressing these issues. Nonetheless, clear boundaries between these cell types remains a challenge and deeper understanding about these lineages are needed.

miloR is a tool designed for complex single-cell datasets[81], which we utilized to form neighborhoods to aggregate gene expression of cells with similar gene expression signatures. Our previous analyses[74] confirmed that neighborhoods were approximately homogeneous in their cell-type composition, providing improved prediction accuracy by addressing sparsity in 10x-type datasets through gene expression aggregation within the same neighborhood. While this aggregation method is beneficial for analyses with sparse datasets, it should be noted that a certain proportion of cells may fail to form neighborhoods (labeled as 'nb_failed' in prediction), leading to information loss for those cell types. Furthermore, if a query dataset contains a very rare subpopulation with limited number of cells, our tool may be unable to form independent neighborhoods of that rare subpopulation and instead merge those cells with the closest resembling cells. Indeed, this was observed with the few amnion cells in the Karvas et al. dataset[76].

Our study has also provided insights into the complexity of stem cell states by comparing the transcriptional profiles of naive and primed hPS cells to early embryonic lineages. The mapping of naive cells to the early epiblast and primed cells to the late epiblast stages resonates with their developmental potential and distinct molecular characteristics. This alignment supports the notion that naive and primed hPS cells mimic distinct developmental time points. The longstanding debate over the ability of human naive and primed stem cells to transition into trophoblast lineages has also been addressed in our study, presenting a nuanced view of this complex process. The identification of trophoblast stem cells cultured under specific conditions mapping to the expected embryonic stages reinforces the notion that, with precise environmental cues, both primed and naive stem cells can be guided into specific lineage pathways. However, the notable presence of amnion and extraembryonic mesodermal cells in primed-derived cell populations underscores the intricate balance and potential for diverse differentiation outcomes inherent in these cells. This finding underscores the necessity for refined cellular markers and rigorous validation strategies to ensure accurate cell lineage fate identification. Although both naive and primed hPS cells can make TLCs, the transcriptional profiles of hPS cell-derived TLCs still differ from their in vivo counterparts. Further, our analysis identifies the same concern for current blastoids: even though they contain the expected cell types, the current blastoids show notable transcriptional differences compared with human blastocysts. From the primed hPS cell-derived TLCs, it appears that part of the problem is related to epigenetic dysregulation as these cells show reduced levels of DNA (cytosine-5)-methyltransferase 3-like (DNMT3L) and long noncoding RNA XIST, which mediated X-chromosome silencing. In this aspect, the naive hPS cell-derived TLCs are more alike the embryo trophoblast lineage. It will be interesting to examine whether starting from an even earlier stem cell state could give added value to embryo models. From that perspective, it is exciting to see that transient conversion to earlier states, such as the 8-cell or morula-like stages could be confirmed in our early embryogenesis prediction tool. We hope this tool will facilitate development of more refined systems to study early human embryogenesis and benchmark these against the human embryo. With the generation of additional in vivo datasets containing postimplantation embryonic or extraembryonic tissues, we aim to continue to expand this reference.

Online content

Any methods, additional references, Nature Portfolio reporting summaries, source data, extended data, supplementary information, acknowledgements, peer review information; details of author contributions and competing interests; and statements of data and code availability are available at https://doi.org/10.1038/s41592-024-02493-2.

References

1. Rossant, J. Why study human embryo development? *Dev. Biol.* **509**, 43–50 (2024).
2. Fu, J., Warmflash, A. & Lutolf, M. P. Stem-cell-based embryo models for fundamental research and translation. *Nat. Mater.* **20**, 132–144 (2020).
3. Rossant, J. & Tam, P. P. L. Opportunities and challenges with stem cell-based embryo models. *Stem Cell Rep.* **16**, 1031–1038 (2021).
4. Posfai, E. et al. Evaluating totipotency using criteria of increasing stringency. *Nat. Cell Biol.* **23**, 49–60 (2021).
5. Posfai, E., Lanner, F., Mulas, C. & Leitch, H. G. All models are wrong, but some are useful: establishing standards for stem cell-based embryo models. *Stem Cell Rep.* **16**, 1117–1141 (2021).
6. Petropoulos, S. et al. Single-cell RNA-seq reveals lineage and X chromosome dynamics in human preimplantation embryos. *Cell* **165**, 1012–1026 (2016).
7. Xiang, L. et al. A developmental landscape of 3D-cultured human pre-gastrulation embryos. *Nature* **577**, 537–542 (2020).
8. Tyser, R. C. V. et al. Single-cell transcriptomic characterization of a gastrulating human embryo. *Nature* **600**, 285–289 (2021).
9. Yanagida, A. et al. Naive stem cell blastocyst model captures human embryo lineage segregation. *Cell Stem Cell* **28**, 1016–1022. e4 (2021).
10. Meistermann, D. et al. Integrated pseudotime analysis of human pre-implantation embryo single-cell transcriptomes reveals the dynamics of lineage specification. *Cell Stem Cell* **28**, 1625–1640. e6 (2021).
11. Yan, L. et al. Single-cell RNA-seq profiling of human preimplantation embryos and embryonic stem cells. *Nat. Struct. Mol. Biol.* **20**, 1131–1139 (2013).
12. Molè, M. A. et al. A single cell characterisation of human embryogenesis identifies pluripotency transitions and putative anterior hypoblast centre. *Nat. Commun.* **12**, 3679 (2021).
13. Weatherbee, B. A. T. et al. Pluripotent stem cell-derived model of the post-implantation human embryo. *Nature* **622**, 584–593 (2023).
14. Rostovskaya, M., Andrews, S., Reik, W. & Rugg-Gunn, P. J. Amniogenesis occurs in two independent waves in primates. *Cell Stem Cell* **29**, 744–759.e6 (2022).
15. Stirparo, G. G. et al. Integrated analysis of single-cell embryo data yields a unified transcriptome signature for the human pre-implantation epiblast. *Development* **145**, dev158501 (2018).

16. Yu, L. et al. Large-scale production of human blastoids amenable to modeling blastocyst development and maternal-fetal cross talk. *Cell Stem Cell* **30**, 1246–1261.e9 (2023).
17. Zheng, Y. et al. Controlled modelling of human epiblast and amnion development using stem cells. *Nature* **573**, 421–425 (2019).
18. Haghverdi, L., Lun, A. T. L., Morgan, M. D. & Marioni, J. C. Batch effects in single-cell RNA-sequencing data are corrected by matching mutual nearest neighbors. *Nat. Biotechnol.* **36**, 421–427 (2018).
19. Radley, A., Corujo-Simon, E., Nichols, J., Smith, A. & Dunn, S.-J. Entropy sorting of single-cell RNA sequencing data reveals the inner cell mass in the human pre-implantation embryo. *Stem Cell Rep.* **18**, 47–63 (2023).
20. Chhabra, S. & Warmflash, A. BMP-treated human embryonic stem cells transcriptionally resemble amnion cells in the monkey embryo. *Biol. Open* **10**, bio058617 (2021).
21. Aibar, S. et al. SCENIC: single-cell regulatory network inference and clustering. *Nat. Methods* **14**, 1083–1086 (2017).
22. Chen, Y., Siriwardena, D., Penfold, C., Pavlinek, A. & Boroviak, T. E. An integrated atlas of human placental development delineates essential regulators of trophoblast stem cells. *Development* **149**, dev200171 (2022).
23. Gallardo, E. F. et al. A multi-omics genome-and-transcriptome single-cell atlas of human preimplantation embryogenesis reveals the cellular and molecular impact of chromosome instability. Preprint at *bioRxiv* https://doi.org/10.1101/2023.03.08.530586 (2023).
24. Gao, H. et al. Suppression of homeobox transcription factor VentX promotes expansion of human hematopoietic stem/multipotent progenitor cells. *J. Biol. Chem.* **287**, 29979–29987 (2012).
25. Yang, R. et al. Amnion signals are essential for mesoderm formation in primates. *Nat. Commun.* **12**, 5126 (2021).
26. Saga, Y. et al. MesP1: a novel basic helix-loop-helix protein expressed in the nascent mesodermal cells during mouse gastrulation. *Development* **122**, 2769–2778 (1996).
27. Street, K. et al. Slingshot: cell lineage and pseudotime inference for single-cell transcriptomics. *BMC Genomics* **19**, 1–16 (2018).
28. Boroviak, T. et al. Single cell transcriptome analysis of human, marmoset and mouse embryos reveals common and divergent features of preimplantation development. *Development* **145**, dev167833 (2018).
29. Nakamura, T. et al. A developmental coordinate of pluripotency among mice, monkeys and humans. *Nature* **537**, 57–62 (2016).
30. Ma, H. et al. In vitro culture of cynomolgus monkey embryos beyond early gastrulation. *Science* **366**, eaax7890 (2019).
31. Bergmann, S. et al. Spatial profiling of early primate gastrulation in utero. *Nature* **609**, 136–143 (2022).
32. Balaton, B. P. & Pasque, V. Human 8-cell-like cells discovered. *Cell Stem Cell* **29**, 347–348 (2022).
33. Töhönen, V. et al. Novel PRD-like homeodomain transcription factors and retrotransposon elements in early human development. *Nat. Commun.* **6**, 8207 (2015).
34. Zheng, Y. et al. Single-cell analysis of embryoids reveals lineage diversification roadmaps of early human development. *Cell Stem Cell* **29**, 1402–1419.e8 (2022).
35. Pham, T. X. A. et al. Modeling human extraembryonic mesoderm cells using naive pluripotent stem cells. *Cell Stem Cell* **29**, 1346–1365.e10 (2022).
36. Li, Z., Korzh, V. & Gong, Z. Localized rbp4 expression in the yolk syncytial layer plays a role in yolk cell extension and early liver development. *BMC Dev. Biol.* **7**, 1–15 (2007).
37. Ross, C. & Boroviak, T. E. Origin and function of the yolk sac in primate embryogenesis. *Nat. Commun.* **11**, 3760 (2020).
38. Stuart, T. et al. Comprehensive integration of single-cell data. *Cell* **177**, 1888–1902.e21 (2019).
39. Hadjiargyrou, M. Mustn1: a developmentally regulated pan-musculoskeletal cell marker and regulatory gene. *Int. J. Mol. Sci.* **19**, 206 (2018).
40. Stelzer, G. et al. The GeneCards suite: from gene data mining to disease genome sequence analyses. *Curr. Protoc. Bioinformatics* **54**, 1.30.1–1.30.33 (2016).
41. Xue, Z. et al. Genetic programs in human and mouse early embryos revealed by single-cell RNA sequencing. *Nature* **500**, 593–597 (2013).
42. Blakeley, P. et al. Defining the three cell lineages of the human blastocyst by single-cell RNA-seq. *Development* **142**, 3151–3165 (2015).
43. Ai, Z. et al. Dissecting peri-implantation development using cultured human embryos and embryo-like assembloids. *Cell Res.* **33**, 661–678 (2023).
44. Zhou, F. et al. Reconstituting the transcriptome and DNA methylome landscapes of human implantation. *Nature* **572**, 660–664 (2019).
45. Aran, D. et al. Reference-based analysis of lung single-cell sequencing reveals a transitional profibrotic macrophage. *Nat. Immunol.* **20**, 163–172 (2019).
46. Kiselev, V. Y., Yiu, A. & Hemberg, M. scmap: projection of single-cell RNA-seq data across data sets. *Nat. Methods* **15**, 359–362 (2018).
47. Ianevski, A., Giri, A. K. & Aittokallio, T. Fully-automated and ultra-fast cell-type identification using specific marker combinations from single-cell transcriptomic data. *Nat. Commun.* **13**, 1246 (2022).
48. Kagawa, H. et al. Human blastoids model blastocyst development and implantation. *Nature* **601**, 600–605 (2022).
49. Okae, H. et al. Derivation of human trophoblast stem cells. *Cell Stem Cell* **22**, 50–63.e6 (2018).
50. Guo, G. et al. Human naive epiblast cells possess unrestricted lineage potential. *Cell Stem Cell* **28**, 1040–1056.e6 (2021).
51. Dong, C. et al. Derivation of trophoblast stem cells from naïve human pluripotent stem cells. *eLife* **9**, e52504 (2020).
52. Bernardo, A. S. et al. BRACHYURY and CDX2 mediate BMP-induced differentiation of human and mouse pluripotent stem cells into embryonic and extraembryonic lineages. *Cell Stem Cell* **9**, 144–155 (2011).
53. Roberts, R. M. et al. Differentiation of trophoblast cells from human embryonic stem cells: to be or not to be? *Reproduction* **147**, D1–D12 (2014).
54. Osnato, A. et al. TGFβ signalling is required to maintain pluripotency of human naïve pluripotent stem cells. *eLife* **10**, e67259 (2021).
55. Soncin, F. et al. Derivation of functional trophoblast stem cells from primed human pluripotent stem cells. *Stem Cell Rep.* **17**, 1303–1317 (2022).
56. Ohgushi, M., Taniyama, N., Vandenbon, A. & Eiraku, M. Delamination of trophoblast-like syncytia from the amniotic ectodermal analogue in human primed embryonic stem cell-based differentiation model. *Cell Rep.* **39**, 110973 (2022).
57. Io, S. et al. Capturing human trophoblast development with naive pluripotent stem cells in vitro. *Cell Stem Cell* **28**, 1023–1039.e13 (2021).
58. Sheridan, M. A. et al. Characterization of primary models of human trophoblast. *Development* **148**, dev199749 (2021).
59. Shannon, M. J. et al. Single-cell assessment of primary and stem cell-derived human trophoblast organoids as placenta-modeling platforms. *Dev. Cell* **59**, 776–792.e11 (2024).
60. Xiao, Z. et al. 3D reconstruction of a gastrulating human embryo. *Cell* **187**, 2855–2874.e19 (2024).
61. Vento-Tormo, R. et al. Single-cell reconstruction of the early maternal-fetal interface in humans. *Nature* **563**, 347–353 (2018).

62. Mazid, M. A. et al. Rolling back human pluripotent stem cells to an eight-cell embryo-like stage. *Nature* **605**, 315–324 (2022).
63. Yoshihara, M. et al. Transient DUX4 expression in human embryonic stem cells induces blastomere-like expression program that is marked by SLC34A2. *Stem Cell Rep.* **17**, 1743–1756 (2022).
64. Yu, L. et al. Blastocyst-like structures generated from human pluripotent stem cells. *Nature* **591**, 620–626 (2021).
65. Liu, X. et al. Modelling human blastocysts by reprogramming fibroblasts into iBlastoids. *Nature* **591**, 627–632 (2021).
66. Fan, Y. et al. Generation of human blastocyst-like structures from pluripotent stem cells. *Cell Discov.* **7**, 81 (2021).
67. Sozen, B. et al. Reconstructing aspects of human embryogenesis with pluripotent stem cells. *Nat. Commun.* **12**, 5550 (2021).
68. Subramanian, A. et al. Gene set enrichment analysis: a knowledge-based approach for interpreting genome-wide expression profiles. *Proc. Natl Acad. Sci. USA* **102**, 15545–15550 (2005).
69. Żylicz, J. et al. Metabolic rewiring underpins human trophoblast induction. Preprint at https://doi.org/10.21203/rs.3.rs-3575549/v1 (2024).
70. Ruan, D. et al. Human early syncytiotrophoblasts are highly susceptible to SARS-CoV-2 infection. *Cell Rep. Med.* **3**, 100849 (2022).
71. Karvas, R. M. et al. Stem-cell-derived trophoblast organoids model human placental development and susceptibility to emerging pathogens. *Cell Stem Cell* **29**, 810–825.e8 (2022).
72. Pedroza, M. et al. Self-patterning of human stem cells into post-implantation lineages. *Nature* **622**, 574–583 (2023).
73. Liu, L. et al. Modeling post-implantation stages of human development into early organogenesis with stem-cell-derived peri-gastruloids. *Cell* **186**, 3776–3792.e16 (2023).
74. Oldak, B. et al. Complete human day 14 post-implantation embryo models from naive ES cells. *Nature* **622**, 562–573 (2023).
75. Hislop, J. et al. Modelling post-implantation human development to yolk sac blood emergence. *Nature* **626**, 367–376 (2024).
76. Karvas, R. M. et al. 3D-cultured blastoids model human embryogenesis from pre-implantation to early gastrulation stages. *Cell Stem Cell* **30**, 1148–1165.e7 (2023).
77. Zheng, G. X. Y. et al. Massively parallel digital transcriptional profiling of single cells. *Nat. Commun.* **8**, 14049 (2017).
78. Dobin, A. et al. STAR: ultrafast universal RNA-seq aligner. *Bioinformatics* **29**, 15–21 (2013).
79. Ouyang, J. F., Kamaraj, U. S., Cao, E. Y. & Rackham, O. J. L. ShinyCell: simple and sharable visualization of single-cell gene expression data. *Bioinformatics* **37**, 3374–3376 (2021).
80. Petrus-Reurer, S. et al. Molecular profiling of stem cell-derived retinal pigment epithelial cell differentiation established for clinical translation. *Stem Cell Rep.* **17**, 1458–1475 (2022).
81. Dann, E., Henderson, N. C., Teichmann, S. A., Morgan, M. D. & Marioni, J. C. Differential abundance testing on single-cell data using k-nearest neighbor graphs. *Nat. Biotechnol.* **40**, 245–253 (2022).

[1]Department of Clinical Science, Intervention and Technology, Karolinska Institutet, and Division of Obstetrics and Gynecology, Karolinska Universitetssjukhuset, Stockholm, Sweden. [2]Department of Integrative Pathophysiology and Therapy, Andalusian Molecular Biology and Regenerative Medicine Centre (CABIMER), Seville, Spain. [3]Stem Cells and Metabolism Research Program, University of Helsinki, Helsinki, Finland. [4]Folkhälsan Research Center, Helsinki, Finland. [5]Department of Mechanical Engineering, University of Michigan, Ann Arbor, MI, USA. [6]Department of Biomedical and Chemical Engineering, Syracuse University, Syracuse, NY, USA. [7]Department of Cell and Molecular Biology, National Bioinformatics Infrastructure Sweden, Science for Life Laboratory, Uppsala University, Uppsala, Sweden. [8]Department of Physiology, Faculty of Medicine, University of Toronto, Toronto, Ontario, Canada. [9]Program in Developmental and Stem Cell Biology, Hospital for Sick Children, Toronto, Ontario, Canada. [10]Department of Cell and Developmental Biology, University of Michigan Medical School, Ann Arbor, MI, USA. [11]Department of Biomedical Engineering, University of Michigan, Ann Arbor, MI, USA. [12]Département de Médecine, Université de Montréal, Montreal, Quebec, Canada. [13]Centre de Recherche du Centre Hospitalier de l'Université de Montréal, Axe Immunopathologie, Montreal, Quebec, Canada. [14]Ming Wai Lau Center for Reparative Medicine, Stockholm Node, Karolinska Institutet, Stockholm, Sweden. ✉e-mail: sophie.petropoulos@ki.se; fredrik.lanner@ki.se

Methods

Ethics declarations

The research complies with all relevant ethical regulations. hES cell line HS975 was previously derived (Swedish Ethical Review Authority: 2011/745:31/3). Donors gave their informed consent for the derivation and subsequent use of the hES cell lines. No compensation was provided to the donating couples.

Differentiation of primed-derived trophoblast-like cells

hES cells growing on hrLN-521 (10 µg ml^{-1}; Biolamina, LN521-02) in NutriStem hPSC XF (Biological Industries, 05-100-1A) were enzymatically dissociated and seeded onto new plates also coated with hrLN-521 at a cell density of 1.84 × 104 cells cm^{-2}. At 24 h after seeding, hPS cells were moved to a 5% CO_2/5% O_2 incubator and differentiated into trophoblastic cells using NutriStem hPSC XF without bFGF (basic fibroblast growth factor) and TGFb (transforming growth factor β) that was supplemented with 10 ng ml^{-1} BMP4 (bone morphogenetic protein 4) (R&D Systems, 314-BP-050e), 1 µM A83-01 (R&D Systems, 2939) and 0.1 µM PD173074 (Sigma-Aldrich, P2499) (BAP treated) according to a previously published protocol[82]. The medium was changed daily during the 4 days of differentiation.

In-house library preparation for scRNA-seq

Cells were dissociated with TrypLE Select (4 min at 37 °C; Thermo Fisher Scientific, 12563011) and deactivated by adding NutriStem hPSC XF and collected in 0.04% BSA (Sigma-Aldrich, A7979) in PBS$^{-/-}$ and used following the cell multiplexing oligo (CMO) labeling for scRNA-seq protocols with feature barcode technology protocol (10x Genomics, CG000391). Viable cells were counted using the NC-200 Nucleocounter (Chemometec) (four CMO samples combined, aiming for 2,000 cells per sample). Chromium Next GEM Single Cell 3′ Reagent Kits v.3.1 (Dual Index) with feature barcode technology for cell multiplexing (10x Genomics, CG000388) was used following the user guide. CMO libraries and transcriptome libraries were sequenced using Illumina NextSeq 2000.

Preprocessing of human scRNA-seq data and gene expression quantification

In-house 10x Genomics multiplexed primed-derived trophoblast scRNA-seq data were processed using the 'cellranger multi' pipeline (v.6.1.1) with default parameters[77]. Published scRNA-seq data were processed using the 'cellranger count' pipeline (v.3.0.0). The STAR aligner (v.2.5.3b)[78] was employed to map reads to the GRCh38 reference genome (v.3.0.0, GRCh38, downloaded from the 10x Genomics website). To minimize differences associated with the sequencing platform and data processing, published Smart-Seq2 datasets and Yan et al.[11] were also remapped to the same reference using the same aligner with default settings. Only uniquely mapped reads were retained for gene expression quantification. Raw read counts were further estimated using rsem-calculate-expression from the RSEM tool (v.1.3.0), with the option of '--single-cell-prior'[83]. Datasets without a note indicating 'reprocessed' in Supplementary Data 9 were based on the previously processed expression matrix reported in their original publication.

Preprocessing of scRNA-seq data and gene expression quantification for marmoset monkeys (*Callithrix jacchus*) and cynomolgus macaques (*Macaca fascicularis*)

The scRNA-seq transcriptomes of marmoset embryos were sourced from Boroviak et al.[28] and Bergmann et al.[31]. Expression matrices were obtained from https://github.com/Boroviak-Lab/SpatialModelling. Cells derived from maternal material were excluded from the analysis. For cynomolgus macaques, embryonic scRNA-seq transcriptomes were downloaded from Nakamura et al.[29], Ma et al.[30] and Yang et al.[25]. Nakamura et al.[29] data were reprocessed and remapped using STAR (v.2.5.3b) with the reference genome 'Macaca_fascicularis_5.0.96' from Ensembl[84], which is used in Yang et al.[25]. Gene expression was quantified using RSEM (v.1.3.0) with cell annotations downloaded from the original publications. Ma et al.[30] data were reprocessed and remapped using Drop-seq tool (v.2.5.1, https://github.com/broadinstitute/Drop-seq) with the same reference genome. Cell annotations for Yang et al.[25] were downloaded from http://www.nhp-embryo.net, with raw reads kindly provided by the authors.

Quality control and normalization

To filter out low-quality cells, we implemented cutoffs based on the number of expressed genes (nGene) and the percentage of mitochondrial genes (percent.mito). For Smart-Seq2 datasets, high-quality cells had at least 2,000 nGene and a percent.mito of less than 0.125. For 10x datasets and other datasets, the cutoffs were determined from original publication or in cases where too few nGene or too high percent.mito was observed, the cutoff was further determined based on the general distribution of nGene and percent.mito. An upper limit for the number of nGene was set to prevent doublets in 10x datasets. Detailed parameters used in quality control for each dataset are listed in the Supplementary Data 9.

After quality control and the exclusion of mitochondrial genes, genes with expression in at least five cells were selected and assessed separately for each dataset. Subsequently, we calculated log-normalized counts using the deconvolution strategy implemented by the 'computeSumFactors' function in the R scran package (v.1.14.6)[85], followed by rescaled normalization using the 'multiBatchNorm' function in the R batchelor package (v.1.2.4)[18]. This ensured that the size factors were comparable across batches. The log-transformed normalized expression after rescaling was then utilized for human dataset integration, marker detection and identification of DEGs.

Restoration of previous cell annotations for published datasets

Original cell identities for human embryonic datasets, excluding those from Petropoulos et al.[6], Xiang et al.[7] and Tyser et al.[8], were obtained from their respective original publications. We utilized the most recently published annotation from Meistermann et al.[10] for the Petropoulos et al.[6] dataset in our analysis. In addition, we examined the ICM cells reported by Stirparo et al.[15] These cells showed substantial overlap with the ICM cells reported by Yanagida et al.[9] (Supplementary Fig. 7a). Specifically, 29 cells were clustered into cluster C1, exhibiting higher expression of ICM-specific markers identified by Radley et al.[19] (Supplementary Fig. 7b,c). Consequently, these cells were classified as ICM cells in our analysis for Petropoulos et al.[6]. Using our embryonic reference, we observed misannotated cells from the Xiang et al.[7] dataset, as also reported by Chhabra et al.[20] (Supplementary Fig. 7d) and, as such, we used the annotations provided by Chhabra et al.[20]. In addition, we reclustered the amnion, PriS and epiblast cells from Tyser et al.[8], as reported in Zheng et al.[34]. We examined the reported markers *ISL1*, *DLX5*, *CLDN10* and *TFAP2A* for amniotic ectoderm as identified from spatial sequencing of human gastrula in Xiao et al.[60]. Twenty cells that were previously annotated as either PriS (19) or epiblast (1), were reannotated as amnion cells because they highly expressed amniotic ectoderm markers but had low expression of *TBXT* or *POU5F1* (Supplementary Fig. 7e) (created by the Seurat pipeline with 2,000 top variable genes and 25 top principal components (PCs)). Further, the cross-species integration analysis performed in Yang et al.[25] with the human CS7 data from Tyser et al.[8] displayed that some of the human Adv_Mes cells overlapped with the cynomolgus monkey extraembryonic mesenchyme cells. In agreement with their observation, integration of the CS7 human gastrula together with postimplanted marmoset data[31], we observed that a proportion (53 of 159 cells) of the previously annotated human Adv_Mes cells overlapped with the marmoset stalk cells. As such, 53 cells previously classified as Adv_Mes cells were reannotated as 'extraembryonic mesoderm' cells, using the spatial

data provided for 'Stalk cells' from the postimplanted marmoset[31] (Supplementary Fig. 7f) during cross-species integration (created by the 'RunFastMNN' function with 2,000 top variable genes and 25 top PCs). We then performed a DEG analysis between the remaining Adv_Mes cells and extraembryonic mesoderm cells and observed that the 53 cells displayed intermediate expression for both these lineages, providing additional evidence supporting the reannotation (Supplementary Fig. 7g). Additionally, a total of 330 EVT and 649 STB cells were identified from previously annotated CTB cells in the cynomolgus monkey (*Macaca fascicularis*)[25,29,30], and 51 CTB and 77 STB cells in the marmoset[31] and confirmed by the expression of markers from human CTB, STB and EVTs (Supplementary Fig. 8). TE cells from Ai et al.[43] were selected using the Seurat pipeline (with 2,000 top variable genes and 25 top PCs) to further delineate the CTB, STB and EVT lineages. For datasets lacking cell annotations, we restored annotations based on their source code or descriptions provided in the original publication. All reanalyzed cell annotations were further validated by the marker gene expression reported in the original publication.

Construction of the human embryonic reference

The human embryonic reference was established by integrating published datasets, included six sets of data spanning zygote early embryos, in vitro cultured blastocysts, 3D in vitro cultured human blastocysts up to pregastrulation stages and a CS7 human gastrula. Integration utilized the fastMNN from the batchelor (v.1.6.2) package. The top 4,000 variable genes were selected using the 'SelectIntegrationFeatures' function from the Seurat package. Four out of the six reference datasets were preimplantation datasets. To mitigate voting bias during the 'SelectIntegrationFeatures' function, the top 2,000 variable genes were first selected from the four preimplantation datasets. Subsequently, a combination consideration was applied to the remaining postimplantation dataset and CS7 dataset. The linear merge of batches followed the order of embryo developmental time points in the datasets. After obtaining the MNN-corrected PCA subspace results from the fastMNN calculation, the UMAP dimensional reduction was calculated using the 'umap' function of the uwot package (v.0.1.14) (https://CRAN.R-project.org/package=uwot), employing the top 50 MNN-corrected PCA subspace. The entire dataset was clustered using the Leiden algorithm ('RunLeiden' function from the Seurat package)[86], utilizing the same neighborhood graph constructed from the corrected PCA subspace. In epiblasts belonging to clusters C1 and C10, 12 were identified as early and late epiblasts, respectively. Primitive endoderm cells were split as early (clusters C1 and C22) and late hypoblasts (cluster C11), respectively (Extended Data Fig. 1b–d). Throughout this process, the grand mean values (grand.centers) values, singular value decomposition results from MNN corrections, variation along the batch vectors, UMAP model and cell clustering were recorded for query dataset projection and identity prediction.

Identification of marker genes and regulatory activity of transcription factors within human embryonic datasets

Lineage marker genes were identified using the 'FindAllMarkers' function with default parameters, with adjusted *P* value cutoff at 0.05. To identify the markers conserved in each lineage of the primate, marker detection was performed within each species and *P* values were combined using 'stouffer' function from poolr package (v.1.1-1)[87] and followed by adjustment. A gene was considered conserved if its expression, with an adjusted *P* value of less than 0.05, was similar in all species. If the gene with an adjusted *P* value of less than 0.05 was highest in only one species' lineage, but not similarly the highest in other two species corresponding lineage, it was considered a species-specific lineage marker gene. The categories hypoblast, DE and YSE are referred to as 'Endoderm', while preimplantation TE, CTB, STB and EVT are grouped as 'TEs'. Additionally, 'ExE_Mech', 'Stalk' and 'ExE_Mes' are consolidated as the 'ExE_Mes_stalk' group, representing the extraembryonic lineage. Adv_Mes and axial mesosderm (Axial_Mes) from humans have been excluded from the mesoderm groups due to their similarity with extraembryonic lineages or distinction from the main mesoderm. 'EmDisc' from marmoset has been included in the epiblast group as the majority of them overlap with the epiblast. Pseudotime trajectory was computed using the R package slingshot (v.2.6.0)[27], facilitating computation of lineage structures in a low-dimensional space. In summary, precomputed cell embeddings and annotations obtained from a human embryonic reference served as input for the 'slingshot' function. The start cluster was set to 'zygote', followed by the application of the 'slingPseudotime' function to infer individual pseudotime. The cells, categorized into prelineages (zygote, 2–4 cell, 8 cell, morula and E5 prelineage), ICM, epiblast, hypoblast, TE and CTB, were utilized to infer the main trajectories. The 'DynamicHeatmap' function from the R package SCP (v.0.5.6, available at https://github.com/zhanghao-njmu/SCP) was employed to identify transcriptional factor genes significantly associated with the pseudotime in the three main trajectories start from the morula stage. Batch-corrected gene expression from six human embryonic datasets was initially calculated using the 'mnnCorrect' function from the batchelor package. The resulting expression profiles were then utilized to identify regulatory modules by inferring coexpression with transcription factors through the 'pyscenic grn--method grnboost2' command. Each coexpression module served as input for *cis*-regulatory motif analyses conducted by running 'pyscenic ctx' with the following motif collections: 'hg38__refseq-r80__10kb_up_and_down_tss.mc9nr.feather', 'hg38__refseq-r80__500bp_up_and_100bp_down_tss.mc9nr.feather' and 'motifs-v9-nr.hgnc-m0.001-o0.0.mod.tbl'[21]. Subsequently, the area under the curve values for each regulon were computed using 'pyscenic aucell'. The top five valid regulons were further selected by requiring regulon activity in more than 1% of total cells and an average area under the curve value exceeding 0.05 for cells belonging to the same lineages.

Cross-species integration

Integration of human datasets with cynomolgus and marmosets data included following steps. First, cynomolgus gene IDs were converted to human gene symbols using the Ensembl ortholog list[88]. Marmoset genes were merged based on shared gene names within the human dataset. Subsequently, rescaled normalization using 'multiBatchNorm' was performed for each species. Cells from Yang et al.[25] were down sampled to 2,000. The top 3,500 variable genes for cynomolgus and marmosets were selected using 'SelectIntegrationFeatures' function, and cross-checked with the top variable genes used in the human embryo reference to confirm overlapping genes amongst all three species. From the 14,978 genes shared between the three species, the 6,005 top variable genes were identified. Of these, 544 or 1,597 genes were identified as the top variable genes in all three species or in any two species, respectively. Additionally, the top 500 species-unique variable genes were included, resulting in a final selection of 3,641 genes for the integration of all three species. To preserve the specificity of each individual species while emphasizing commonalities, the 'mnnCorrect' function from the batchelor package was used to calculate batch-corrected expression within each species separately. Batch-corrected expression of the three species, which removed within-species batch differences, served as input for the 'FindIntegrationAnchors' and 'IntegrateData' functions from the Seurat package for integration. Subsequently, the top 20 PCs were calculated using the 'RunPCA' function and utilized for UMAP dimensional reduction with the 'RunUMAP' function.

For data integration of preimplantation blastoids with in vitro cultured postimplantation cynomolgus monkey embryos (wild-type, day 14)[25], normalization was performed separately for each dataset. Each human blastoid dataset and cynomolgus monkey dataset were integrated using the 'RunfastMNN' function (wrapped in the R SeuratWrappers package (v.0.3.0)) with 2,000 anchor features and the top

25 PCs. The resulting components were used for UMAP dimensional reduction with the 'RunUMAP' function.

Projection of query dataset on human embryonic reference

To project the query dataset without influencing original dimensional reduction of reference dataset, the following steps were taken:

(1) Normalization: when incorporating a query dataset, it is rescaled to the lowest coverage batch of the reference dataset[9]. The rescaling factor used for the reference dataset is also applied to the query dataset;

(2) MNN correction and PCA projection: implementing MNN correction to remove the batch effect assumes that the presence of MNNs defines the most similar cells of the same type across batches and that the batch effect is almost orthogonal to the biological subspace. The sample size of the query dataset and the value of *K*, which defines the number of neighbors checked, can influence the prediction of MNN pairs. Therefore, we tested the accuracy of MNN pairs originating from the same reference lineages under different parameters (Extended Data Fig. 4a,b). Using the dataset from Ai et al.[43], containing the largest number of embryonic cells, as our test dataset, we examined the *F*-score values of corrected MNN pairs under different values of *K* and downsampling sizes, as well as the processing time (Extended Data Fig. 4b). Accordingly, the query dataset was divided into several 200 subsamples and the default value of *K* was set to 30, except when the number of query samples was less than 50, in which case *K* was set to 5. In addition, each sample was randomly selected five times to form different subsamples to prevent bias introduced by downsampling. For the entirety of the MNN calling process, the 'findMutualNN' function from the batchelor R package was employed on cosine normalization values between the query dataset and each reference dataset. In our reference dataset, distinguishing between the two cell populations, TE and amnion, poses challenges due to their gene expression similarities. To further enhance accuracy, query cells assigned to both amnion and TE reference MNN pairs were discarded from downstream analysis to circumvent inaccurate calculation based on the cells with ambiguous signatures. Instead, only cells with clear signatures for either amnion or TE were retained, thus better distinguishing cell types. In addition, MNN pairs with low correlation coefficients and those belonging to reference lineages where the top 20 correlation coefficients were less than 0.5 were filtered out due to poor quality. Subsequently, the query cosine-normalized data underwent removal of the same grand mean values (grand.centers) of each gene from reference dataset construction. This was followed by a dot product calculation with left singular vectors from singular value decomposition in the reference construction and removing variation along the reference batch correction vector (orthogonalization) using the internal functions '.orthogonalize_other' and '.center_along_batch_vector', previously wrapped in the 'fastMNN' function, to place the query dataset into the same corrected batch-corrected PCA space as the reference datasets. As described in the original paper[18], cell-specific batch correction vectors were calculated based on identified MNN pairs and a further batch correction on PCA space was performed using internal functions '.compute_correction_vectors' and '.adjust_shift_variance', previously wrapped in the 'mnnCorrect' function from batchelor (v.1.6.2)[18];

(3) UMAP calculation: after obtaining batch-corrected PCA subspace results for the query dataset, 2D UMAP projections were calculated using the 'umap_transform' function based on the previously mentioned reference UMAP model.

To filter out nonrelated cells, a Spearman correlation was calculated between the query data and the reference dataset using cosine normalization values. To set the threshold for filtering irrelevant cells, processed expression files from unrelated datasets, including five scRNA-seq datasets from human pancreas, macrophage, fetal kidney development and liver tissues, were downloaded from https://cblast.gao-lab.org/ to test the correlation coefficient with human embryonic reference cells[89–93]. In our analysis, cells with a mean top correlation coefficient (calculated within top 20 correlated reference cells) less than 0.5 were considered nonrelated. In addition, before the entire projection calculation, raw counts for cells from 10x datasets stratified by different time point or treatment with similar expression patterns were aggregated within neighborhood nodes, as calculated by miloR package (v.1.2.0)[81]. This aggregation enhances our MNN calculation and correlation calculation. 'prop' were set to 0.15 for 'makeNhoods' function from miloR package based on the performance testing results (Extended Data Fig. 4a,b).

Prediction of cell identities

To predict cell identities, we first trained a SVM classifier for each lineage in latent space. Specifically, the embryonic reference dataset was split into training and testing data using fivefold cross-validation. Within each fold, we performed a grid search to find the best hyperparameters by tuning the *C* and gamma parameters of the radial basis function kernel (svmRadial). The optimal combination of hyperparameters was selected based on the 'Kappa' metric value. The R packages caret (v.6.0-88)[94] and e1071 (v.1.7-13) (https://cran.r-project.org/web/packages/e1071/) were used here. For the query dataset, we then transformed the data into the same *N* dimensions as the reference using the 'umap_transform' function and was predicted utilizing the best-trained models for that dimension. Cells with the highest prediction probability no less than 0.5 were assigned to the corresponding reference lineages. Cells with the highest prediction probability lower than 0.5 were labeled as 'ambiguous'. Additionally, based on the assumption that MNN pairs represent the most similar cells of the same type across batches, predicted lineages without support from MNN pairs were labeled as 'ambiguous', possibly due to inaccurate UMAP transformation or batch correction for query cells. For query datasets aggregated with neighborhood nodes, cells contributing to the neighborhood were assigned the same predicted annotation as that for the neighborhood. Cells with multiple predicted lineages were reported by the highest prediction probability. Cells that failed to form a neighborhood during miloR calculation were labeled as 'nb_failed'.

To evaluate the dimensionality of the latent space that yields the best classifier performance, the original 50-dimensional PCA-corrected space of the reference dataset was also transformed into 2- (as used for visualization), 5-, 10- and 20-dimensional UMAP latent space. We evaluated the overall performance for each best model trained on $n = 2, 5, 10$ and 20 UMAP latent space or original $n = 50$ in PCA space. The given 11 embryonic datasets were transformed into the same *N* dimensions as the reference dataset using the 'umap_transform' function. The best models trained were then used to evaluate overall performance. Transforming into a 20-dimensional latent space yielded the best performance based on the kappa values of the predictions for all embryonic data (Extended Data Fig. 4c).

The R packages SingleR (v.1.4.1)[45], scmap (v.1.12.0)[46] and ScType (v.6db9eef)[47] with default settings were used to compare the cell type annotations (Extended Data Fig. 4d). Gene expression and rescaled log-transformed normalization matrices of all six embryonic reference datasets were merged into one input reference dataset for SingleR, or served as a separate reference list for the 'scmapCluster' function from scmap. The top 15 identified lineage marker genes were used as the reference input for the 'sctype_score' function from ScType.

Module score calculation

The predicted lineage scores for each cell were calculated using the 'AddModuleScore' function from Seurat package, incorporating the top 15 identified lineage marker genes.

Detection of top DEGs among amnion, PriS and ExE_Mes cells and TE

The 'FindMarkers' function utilizing the two-sided 'wilcox' test from the Seurat package was employed for differential expression analysis.

Gene expression of amnion, PriS and extraembryonic cells from Tyser et al.[8] were compared with TE cells from Petropoulos et al.[6], Yanagida et al.[9], Meistermann et al.[10] and Xiang et al.[7]. The TE cells from Xiang et al.[7] were categorized into preimplantation TE and postimplantation CTB, STB and EVT. All TE populations were compared with amnion, PriS or ExE_Mes cells. Since cells of late lineages and TE lineages were not from the same dataset, batch difference could influence DEG detection. For a gene to be considered truly differentially expressed, it had to meet four additional criteria: (1) average expression level in upregulated lineages greater than 10; (2) $\log_2$(fold change) greater than 0.25 in all five comparisons; (3) adjusted *P* value less than 0.05 in at least four comparisons; and (4) the percentage of cells expressing the gene in the highly expressed group greater than 50% and the percentage of cells expressing the gene in the lowly expressed group less than 25%. To ensure consistency, DEGs located on the sex chromosome were excluded from analysis, considering only the male embryo included in Tyser et al.[8].

Detection of DEGs between naive/primed-derived TLC and preimplantation embryonic TE

The gene expression profiles of predicted naïve and primed TLCs were compared with TE cells obtained from studies by Petropoulos et al.[6], Yanagida et al.[9], Meistermann et al.[10] and Xiang et al.[7], specifically focusing on preimplantation TE cells (E6 to E7). When comparing all TE populations, considering that the nonembryonic datasets were all generated on 10x platforms, for a gene to be considered truly differentially expressed, it needed to meet four additional criteria: (1) $\log_2$(fold change) >0.25 in at least three comparisons; (2) adjusted *P* value <0.05 in at least three comparisons; (3) adjusted merged *P* values combined by 'stouffer' function less than 0.05; and (4) the percentage of cells expressing the gene in the highly expressed group greater than 50% and percentage of cells expressing the gene in the lowly expressed group less than 25% in at least three comparisons.

Detection of DEGs among blastoid-derived ELC, HLC and TLC versus corresponding preimplantation embryonic lineages

Gene expression profiles of ELC, HLC and TLC from studies by Yanagida et al.[9], Kagawa et al.[48] and Yu et al.[64] were compared with preimplantation embryonic related lineage cells from studies including Petropoulos et al.[6], Yanagida et al.[9], Meistermann et al.[10] and Xiang et al.[7], respectively. When comparing blastoid lineage-like cells with embryonic reference cells, given the limited number of reference cells for the preimplantation hypoblast in studies by Yanagida et al.[9], Meistermann et al.[10] and Xiang et al.[7] (14, 2 and 7 cells, respectively), hypoblast cells from Meistermann et al.[10] were excluded in the reference comparison. Comparisons between HLC and primitive endoderm cells from Yanagida et al.[9] and Xiang et al.[7] *P* values were considered significant. To be considered truly differentially expressed, a gene had to meet three additional criteria, including: (1) $\log_2$(fold change) >0.25 in at least three comparisons; (2) having an adjusted *P* value <0.05 in at least three comparisons; and (3) adjusted merged *P* values combined by 'stouffer' function <0.05. GSEA was performed using the 'GSEA' function from the clusterProfiler package (v.3.18.1)[95], with the average $\log_2$(fold change) from four comparisons with embryonic lineages as input. WikiPathway annotations and gene sets for GSEA were downloaded from the Molecular Signatures Database[68,96]. Significantly regulated WikiPathways were identified as those with a Benjamini–Hochberg-adjusted *P* value less than 0.05.

Extension of human embryonic reference

Two additional datasets were included: spatial transcriptomics from a CS8 human embryo[60] and 10x-sequenced single-cell transcriptomes of STB, EVT and villous CTB from first-trimester placentas[61]. These were added to the original six reference datasets to test the extension capabilities of our reference construction strategy. Since the sequencing depth of the spatial transcriptomics and 10x single-cell transcriptomes were 130 and 20 times lower, respectively, compared with the six non-droplet-based datasets, we aggregated the raw gene expression of the CS8 spatial transcriptomics[60] two times using the same strategy for sparse query datasets by miloR. Similarly, for the 10x-sequenced dataset, one-time aggregation was employed for the first-trimester placentas cells. After aggregation, reference construction followed the same normalization, MNN correction and UMAP reduction steps as for our original reference construction, utilizing the top 4,500 variable genes and 50 PCs. Query datasets, including TLCs derived from naive and primed hPS cells and organoids derived from the first trimester[59], were projected onto this extended reference following the same processing steps as for the original reference.

Statistics and reproducibility

On the basis of the prediction performance, the downsampling sample size in Fig. 2a was determined as 200. No data were excluded from the analyses. The samples were not randomized unless specified in Extended Data Figs. 3a,d and 8a,b,d. Cells from Yang et al.[25] were downsampled to 2,000 in Extended Data Fig. 3a. Cells more than 200 cells were downsampled to 200 in Extended Data Figs. 3d and 8a,b,d.

Web interface

A shiny app generated by shinyCell[79], which includes the above integration, as our early embryogenesis prediction tool can be browsed at http://petropoulos-lanner-labs.clintec.ki.se.

Reporting summary

Further information on research design is available in the Nature Portfolio Reporting Summary linked to this article.

Data availability

Datasets utilized in this study were obtained as summarized in Supplementary Data 9. These include 13 human embryonic datasets covering various stages of embryogenesis (Yan et al.[11] (GSE36552), Xiang et al.[7] (GSE136447), Tyser et al.[8] (E-MTAB-9388), Yanagida et al.[9] (GSE171820), Meistermann et al.[10] (PRJEB30442), Zhou et al.[44] (GSE109555), Xue et al.[41] (GSE44183), Molè et al.[12] (E-MTAB-8060), Ai et al.[43] (PRJCA017779), Blakeley et al.[42] (GSE66507), Petropoulos et al.[6] (E-MTAB-3929), Xiao et al.[60] (HRA005567) and Vento-Tormo et al.[61] (E-MTAB-6701)). Additionally, we included seven preimplantation blastoid models (Yu et al.[64] (GSE150578), Liu et al.[65] (GSE156596), Kagawa et al.[48] (GSE177689), Fan et al.[66] (GSE158971), Sozen et al.[67] (GSE178326), Yu et al.[16] (GSE210962) and Yanagida et al.[9] (GSE171820)); seven post-implantation stem cell-based models (Karvas et al.[76] (GSE226794), Hislop et al.[75] (GSE247111), Weatherbee et al.[13] (GSE218314), Oldak et al.[74] (GSE239932), Pedroza et al.[72] (GSE208195), Liu et al.[73] (GSE232861) and Ai et al.[43] (PRJCA017779)); three studies involving naive cells giving rise to TLCs (Io et al.[57] (GSE167924), Guo et al.[50] (GSE166422) and Osnato et al.[54] (E-MTAB-10018)); three studies using primed human embryonic cells giving rise to TLCs (one generated in house (GSE254641), Soncin et al.[55] (GSE182791) and Ohgushi et al.[56] (GSE196365)); two studies analyzing 8CLCs (Mazid et al.[62] (CNP0001454) and Yoshihara et al.[63] (E-MTAB-10581)); one study with a PASE model (Zheng et al.[17] (GSE134571)); and one study from human trophoblast organoids (Shannon et al.[59] (GSE216244)). Furthermore, we included two embryonic datasets from *Callithrix jacchus* (marmoset) (Bergmann et al.[31] (E-MTAB-9367) and Boroviak et al.[28] (E-MTAB-7078)) and three embryonic datasets from *Macaca fascicularis* (crab-eating macaque) (Nakamura et al.[29] (GSE74767), Ma et al.[30] (GSE130114) and Yang et al.[25] (GSE148683)). Yanagida et al.[9] 2021 and Ai et al.[43] both contain embryonic and stem cell model data. The processed dataset, including predicted annotations, UMAP and sorted cell counts, can be

retrieved from https://petropoulos-lanner-labs.clintec.ki.se/dataset.download.html. Source data are provided with this paper.

Code availability

All original code has been deposited and is available via Zenodo at https://zenodo.org/records/12189592 (ref. 97) with a GPL-3.0 license for all versions. Any additional information required to reanalyze the data reported in this work paper is available from the lead contact upon request.

References

82. Amita, M. et al. Complete and unidirectional conversion of human embryonic stem cells to trophoblast by BMP4. *Proc. Natl Acad. Sci. USA* **110**, E1212–E1221 (2013).
83. Li, B. & Dewey, C. N. RSEM: accurate transcript quantification from RNA-seq data with or without a reference genome. *BMC Bioinform.* **12**, 1–16 (2011).
84. Cunningham, F. et al. Ensembl 2019. *Nucleic Acids Res.* **47**, D745–D751 (2019).
85. Lun, A. T. L., McCarthy, D. J. & Marioni, J. C. A step-by-step workflow for low-level analysis of single-cell RNA-seq data with Bioconductor. *F1000Res.* **5**, 2122 (2016).
86. Traag, V. A., Waltman, L. & van Eck, N. J. From Louvain to Leiden: guaranteeing well-connected communities. *Sci. Rep.* **9**, 5233 (2019).
87. Cinar, O. & Viechtbauer, W. The poolr package for combining independent and dependent *P* values. *J. Stat. Softw.* **101**, 1–42 (2022).
88. Cunningham, F. et al. Ensembl 2022. *Nucleic Acids Res.* **50**, D988–D995 (2022).
89. Bian, Z. et al. Deciphering human macrophage development at single-cell resolution. *Nature* **582**, 571–576 (2020).
90. Enge, M. et al. Single-cell analysis of human pancreas reveals transcriptional signatures of aging and somatic mutation patterns. *Cell* **171**, 321–330.e14 (2017).
91. Hochane, M. et al. Single-cell transcriptomics reveals gene expression dynamics of human fetal kidney development. *PLoS Biol.* **17**, e3000152 (2019).
92. Cao, Z.-J., Wei, L., Lu, S., Yang, D.-C. & Gao, G. Searching large-scale scRNA-seq databases via unbiased cell embedding with Cell BLAST. *Nat. Commun.* **11**, 3458 (2020).
93. MacParland, S. A. et al. Single-cell RNA sequencing of human liver reveals distinct intrahepatic macrophage populations. *Nat. Commun.* **9**, 4383 (2018).
94. Kuhn, M. Building predictive models in R using the caret package. *J. Stat. Softw.* **28**, 1–26 (2008).
95. Yu, G., Wang, L.-G., Han, Y. & He, Q.-Y. clusterProfiler: an R package for comparing biological themes among gene clusters. *OMICS* **16**, 284–287 (2012).
96. Liberzon, A. et al. The Molecular Signatures Database (MSigDB) hallmark gene set collection. *Cell Syst.* **1**, 417–425 (2015).
97. Code/docker for human early embryo reference and projection tool. *Zenodo* https://zenodo.org/records/12189592 (2024).

Acknowledgements

We thank members of the laboratories of F.L. and S.P. for discussions. This work was supported by the Swedish Research Council (2023-02582, F.L. and 2016-01919, S.P.), Ragnar Söderberg Foundation (M67/13, F.L.), Ming Wai Lau Center for Reparative Medicine (F.L.), Center for Innovative Medicine (F.L.), Wallenberg Academy Fellow (KAW 2016.0121, F.L.), Vinnova (2021-02695, F.L.), Swedish Society for Medical Research (S16-0039, S.P.), Emil och Wera Cornells Stiftelse (093-2019/2020, S.P.), Natural Sciences and Engineering Research Council of Canada Discovery Grant (RGPIN-2019-05423, S.P), The Canadian Institutes of Health Research (PJT-178082, S.P. and J.R.), Päivikki and Sakari Sohlberg Foundation (J.W.) and Sigrid Jusélius Foundation (J.W.). S.P. holds the Canada Research Chair in Functional Genomics in Reproduction and Development (950-233204). We thank E. Mahammadov, R. Yang and A. Goedel, S. Srinivas, M. Molè, M. Zernicka-Goetz, A. Scialdone, Y. Yi, Z. Ai, T. Li, L. Yu and Y. Yuan for sharing with us their processed gene expression matrices and corresponding published annotation from their work. The computations and data handling were partially enabled by resources in project NAISS 2023/22-988 and NAISS 2023/23-490 provided by the National Academic Infrastructure for Supercomputing in Sweden (NAISS), partially funded by the Swedish Research Council through grant agreement no. 2022-06725.

Author contributions

C.Z., S.P. and F.L. conceived the study with advice from A.P.R. and J.P.S. A.P.R. and J.W. produced the primed-derived TLC, which were sequenced with assistance from L.B.-V. Data analysis was performed by C.Z. with input from S.P., F.L. and Å.K.B. The interpretation of results was performed by C.Z., F.L., S.P., A.P.R., J.P.S., J.W., N.M.O. Y.Z., J.S., R.T., B.C., J.R. and J.F. The manuscript was written by C.Z., J.F., F.L. and S.P., with input from all of the authors.

Funding

Open access funding provided by Karolinska Institute.

Competing interests

J. Fu is an editor of *NPJ Regenerative Medicine*. The other authors declare no competing interests.

Additional information

Extended data is available for this paper at https://doi.org/10.1038/s41592-024-02493-2.

Supplementary information The online version contains supplementary material available at https://doi.org/10.1038/s41592-024-02493-2.

Correspondence and requests for materials should be addressed to Sophie Petropoulos or Fredrik Lanner.

Peer review information *Nature Methods* thanks Manu Setty, and the other, anonymous, reviewer(s) for their contribution to the peer review of this work. Primary Handling Editor: Madhura Mukhopadhyay, in collaboration with the *Nature Methods* team.

https://doi.org/10.1038/s41592-024-02493-2

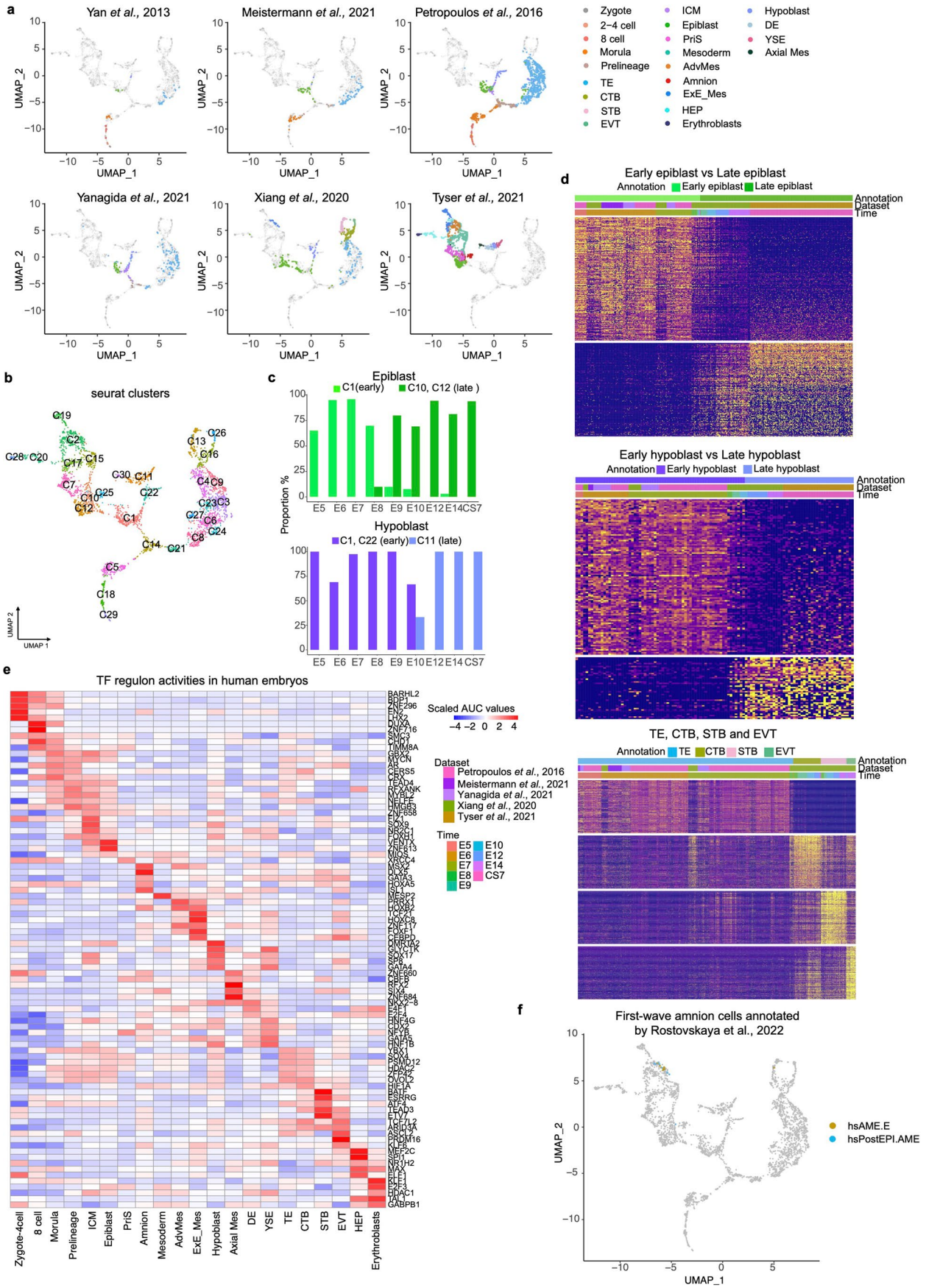

Extended Data Fig. 1 | See next page for caption.

https://doi.org/10.1038/s41592-024-02493-2

Extended Data Fig. 1 | Clusters and regulon activity within the human embryonic reference. a, UMAP projection used in Fig. 1a shown by each embryonic dataset separately, colour of each data point indicates the cell annotations. **b**, Unassigned cluster distribution of UMAP used in Fig. 1a. **c**, Cell distribution in clusters for epiblast and hypoblast cells. **d**, Heatmap showing expression of DEGs between early and late epiblast, early and late hypoblast and DEGs among TE, CTB, STB and EVT. **e**, Heatmap displaying average AUC values of top 5 enriched regulons within each lineage. **f**, Highlighted first-wave amnion cells from Xiang et al. 2020 (based on the annotation from Rostovskaya et al., 2022). Abbreviations, hsPostEPI-AME: intermediates between epiblast and amnion cells; hsAME-E: early amniotic epithelium.

https://doi.org/10.1038/s41592-024-02493-2

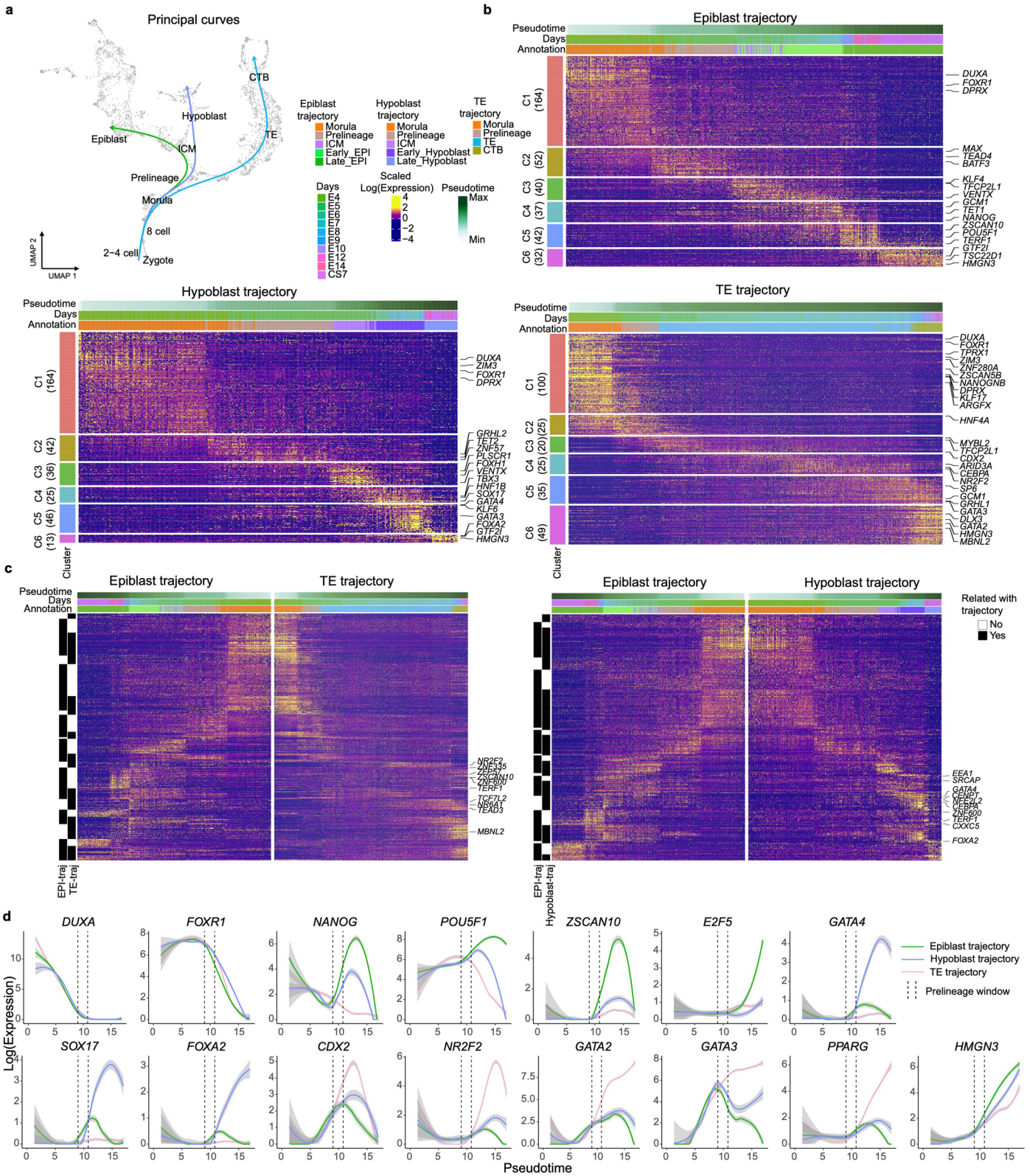

Extended Data Fig. 2 | Transcription factor gene expression along the epiblast, hypoblast, and TE trajectories. a, Principle curves, and trajectories constructed from slingshot. **b**, Heatmap of expression of transcription factor (TF) genes which were significantly related to trajectories pseudotime. Cluster pattern of expression was indicated on the left with numbers indicating the number of TF genes. **c**, Joint heatmap showing expression of TF genes related to epiblast/TE trajectories and epiblast/hypoblast trajectories. The black and white annotation on the left indicated whether corresponding TF were significantly related to pseudotime. **d**, Expression dynamics (pseudotime) of selected transcriptional factor genes along three main trajectories. The confidence interval (error bands, 95%) is indicated by bandwidth. The measure of center and confidence intervals were calculated using the 'loess' function with default parameters in R software. Different trajectories are indicated by colours, respectively.

https://doi.org/10.1038/s41592-024-02493-2

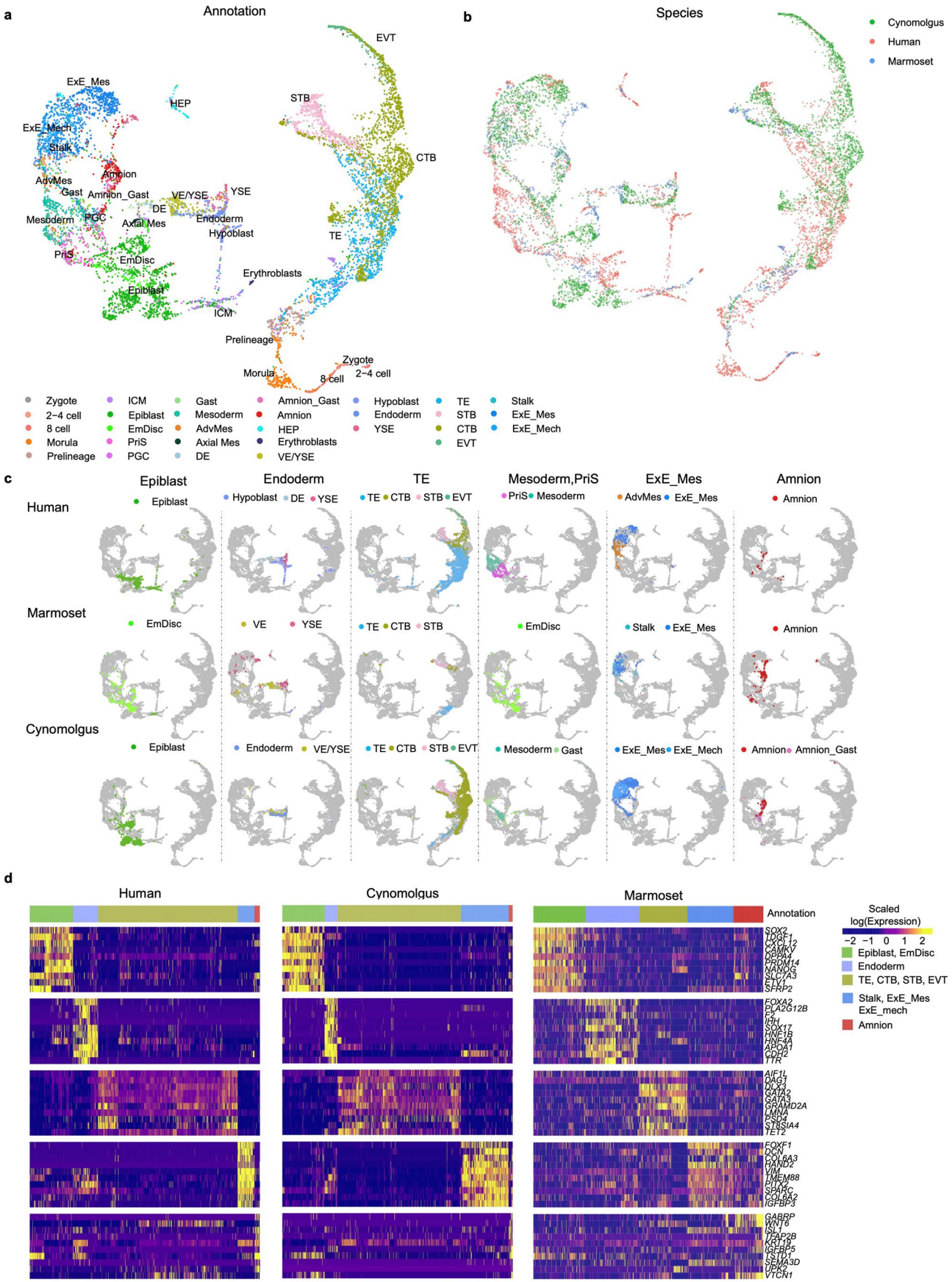

Extended Data Fig. 3 | See next page for caption.

https://doi.org/10.1038/s41592-024-02493-2

Extended Data Fig. 3 | Cross-species integration involving cells from early human, cynomolgus monkey, and marmoset embryos. a, UMAP projection of the integrated datasets from six human, three cynomolgus monkey, and two marmoset embryos. Each data point's colour corresponds to the cell annotations retrieved from each publication. **b**, Similar to (**a**), but the colour represents the species of the data. **c**, Highlights cells from each lineage belonging to their respective species in the cross-species integration. **d**, Expression of the top 10 lineage marker genes conserved in primate species. Abbreviations, ICM: inner cell mass; TE: trophectoderm; CTB: Cytotrophoblast; STB: Syncytiotrophoblast; EVT: Extravillous trophoblast; PriS: primitive streak; AdvMes: advanced mesoderm; DE: definitive endoderm; ExE_Mes:extraembryonic mesoderm; YSE: yolk sac endoderm; HEP: haemato-endothelial progenitors; EmDisc: embryonic disc; VE: visceral endoderm; SYS: secondary yolk sac; Gast: 'Gastrula'; ExE_mech: extraembryonic mesenchyme.

https://doi.org/10.1038/s41592-024-02493-2

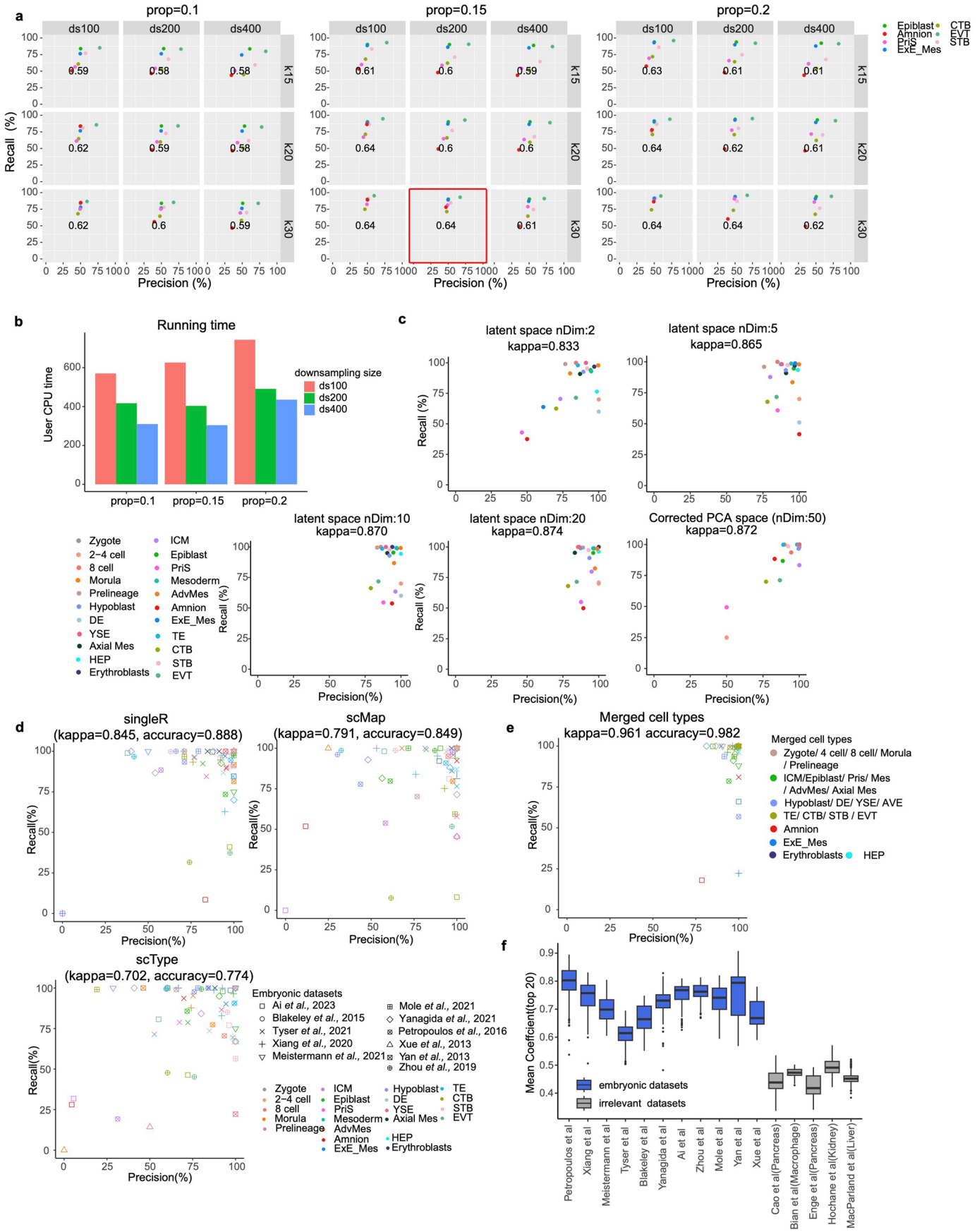

Extended Data Fig. 4 | See next page for caption.

https://doi.org/10.1038/s41592-024-02493-2

Extended Data Fig. 4 | Parameter selection for processing workflow. **a**. Precision and recall ratios for aligned MNN pairs between the Ai et al., 2023 embryonic datasets and reference embryonic datasets under different parameters, including 'prop' (the proportion of randomly sampling during neighbourhood aggregation), 'K' (the number of neighbours considered), and downsampling size. The F-score values are shown on the plot. The colour of each data point represents the cell annotations from the Ai et al., 2023 embryonic dataset. **b**. CPU running time for MNN calculation under different 'prop' values and downsampling sizes. Here, 'K' was arbitrarily set to 30 as we determined this value had minimal influence on running time. **c**. Prediction precision and recall ratios for each cell type from all embryonic datasets using models trained with different numbers of dimensions. The colour of each data point represents the cell types. Performance metrics for the same cell types from different embryonic datasets were averaged. **d**. Prediction precision and recall ratios for each cell type using SingleR, scMap, and ScType. **e**, Prediction precision and recall ratio for merged cell types in the embryonic datasets. The shape and colour of data points indicate queried cell types and data sources, respectively. **f**. Shown the top 20 mean correlation coefficients of each cell from each dataset. The embryonic datasets are coloured blue, while irrelevant datasets are coloured grey. The boxplot rectangles represent the first and third quartiles, with whiskers extending 1.5 times the interquartile range above and below the box. A horizontal line inside the box indicates the median value. Outliers are indicated as dots.

https://doi.org/10.1038/s41592-024-02493-2

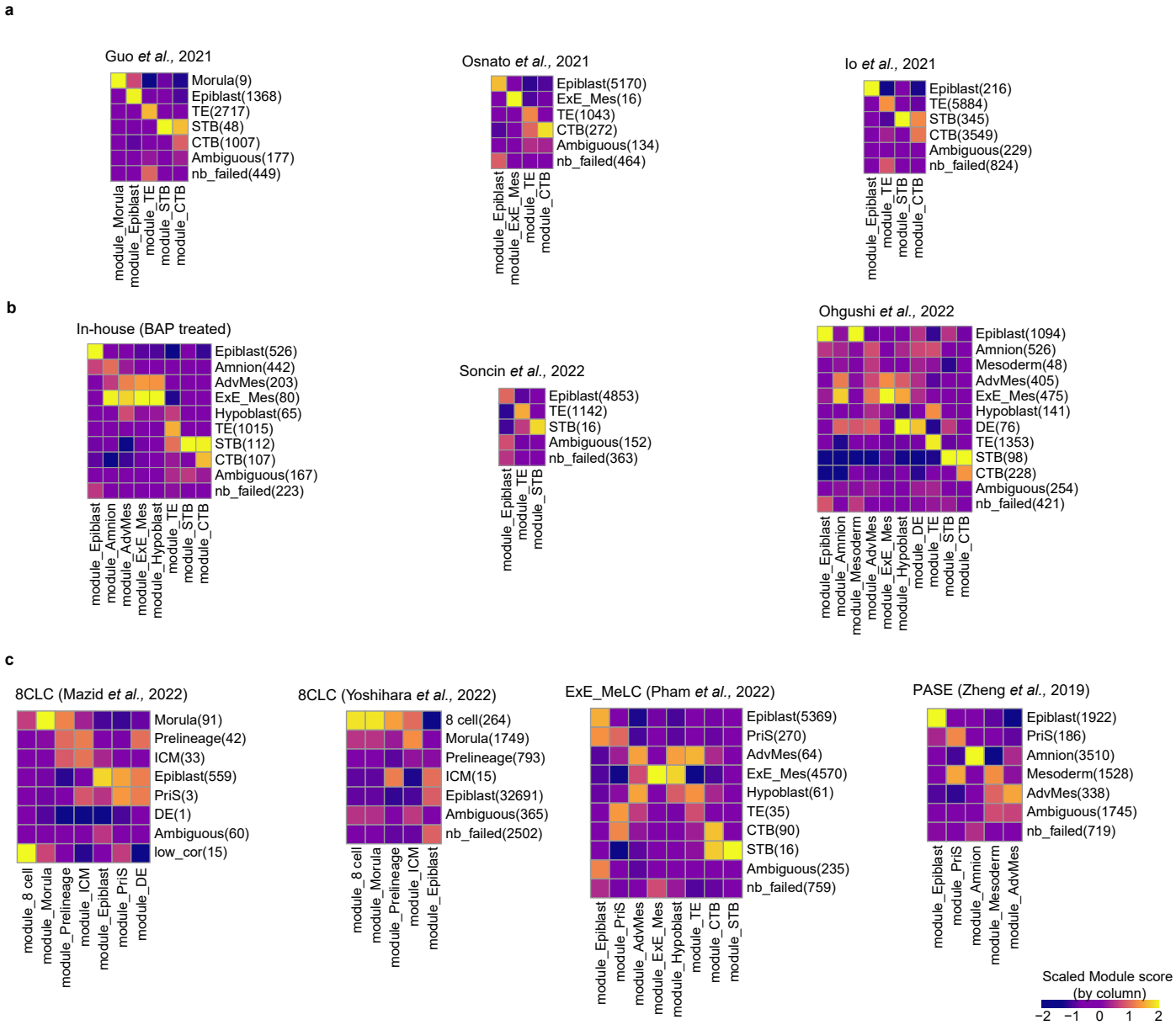

Extended Data Fig. 5 | Module scores of cell models. Module scores of corresponding predicted lineages in three naïve stem cells models (**a**), three primed stem cells models (**b**), two 8-cell-like models, one extraembryonic mesoderm-cell-like model, and PASE models (**c**). Columns represent different lineage models scores, and rows represent predicted lineages for each dataset. The predicted cell numbers are included in parentheses.

https://doi.org/10.1038/s41592-024-02493-2

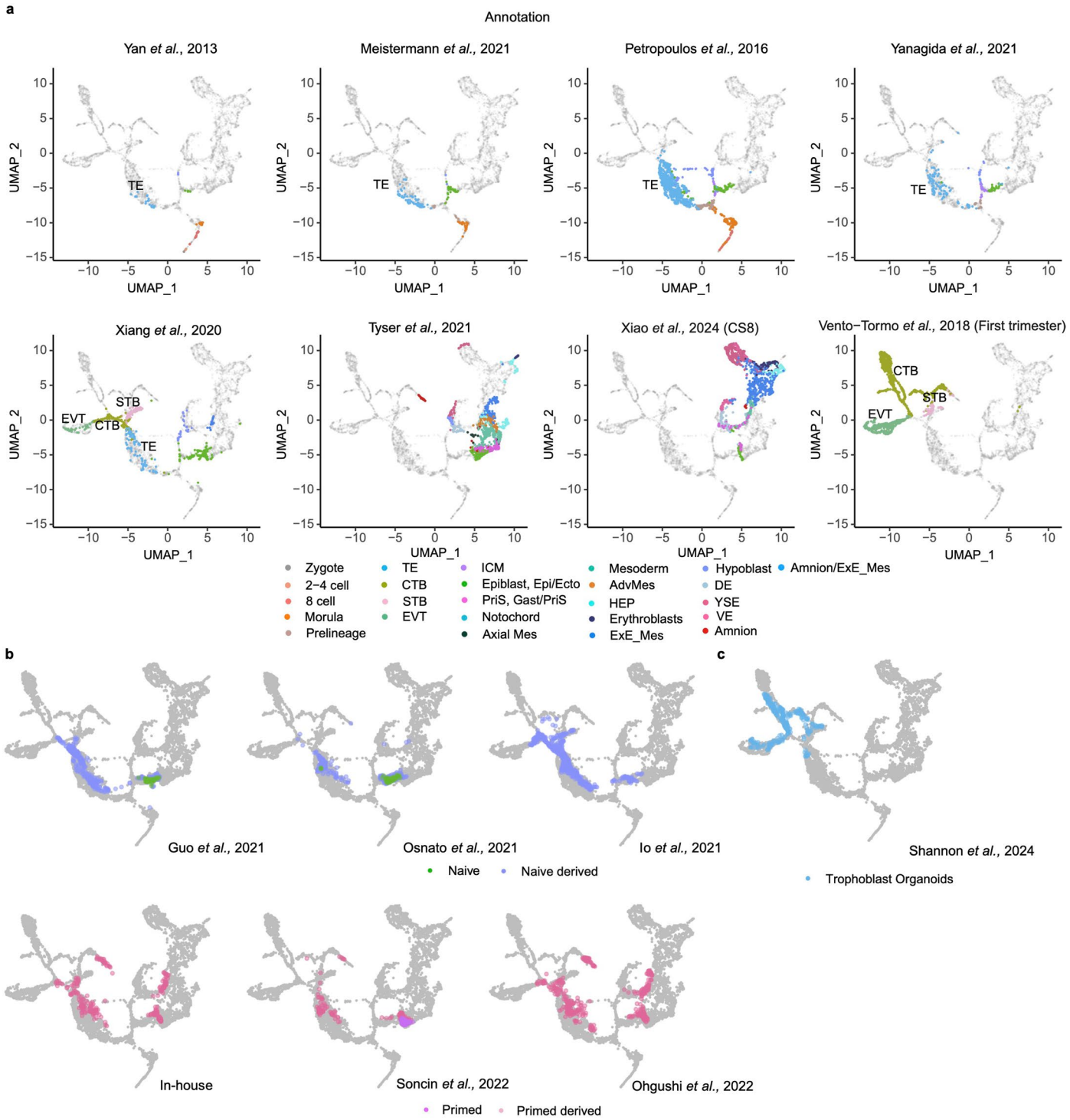

Extended Data Fig. 6 | Extension of the human embryonic reference. **a**, UMAP projection of the integration of eight embryonic datasets including original six embryonic datasets used in Fig. 1, spatial transcriptomics from a Carnegie stage (CS) 8 human embryo (Xiao et al., 2024) and 10X-sequenced single-cell transcriptomes of STB, EVT, and villous CTB from first-trimester placentas (Vento-Tormo et al., 2018). Colour of each data point indicates the cell annotations. **b**, Projection of six datasets that use naïve or primed cells to model TLCs. The colour of each data point represents whether the cells (neighbourhood nodes) are naïve, primed, or their derived cells. **c**. Projection of organoids derived from the first trimester (Shannon et al., 2024).

https://doi.org/10.1038/s41592-024-02493-2

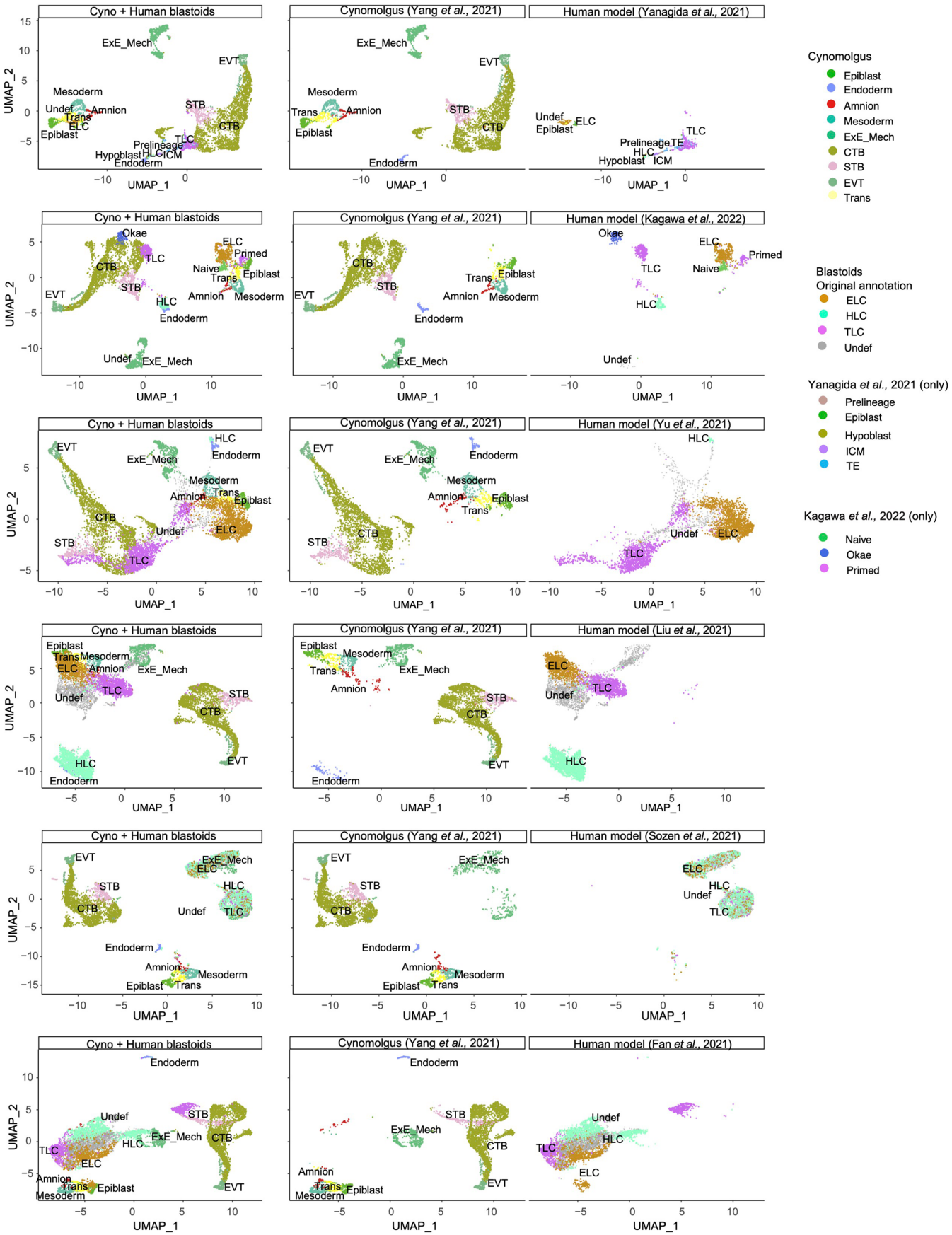

Extended Data Fig. 7 | UMAP projection of Mutual Nearest Neighbours (MNN) cross-species integration of blastoid models and cynomolgus macaque at Day 14. Embryonic cells from Yanagida et al. and naïve, primed, and Okae cells from Kagawa et al. were also included in the integration. Overlay and separation by source of datasets is shown on the left and right, respectively. Colour corresponds to (Yang et al., 2021), coloured by cell type.

https://doi.org/10.1038/s41592-024-02493-2

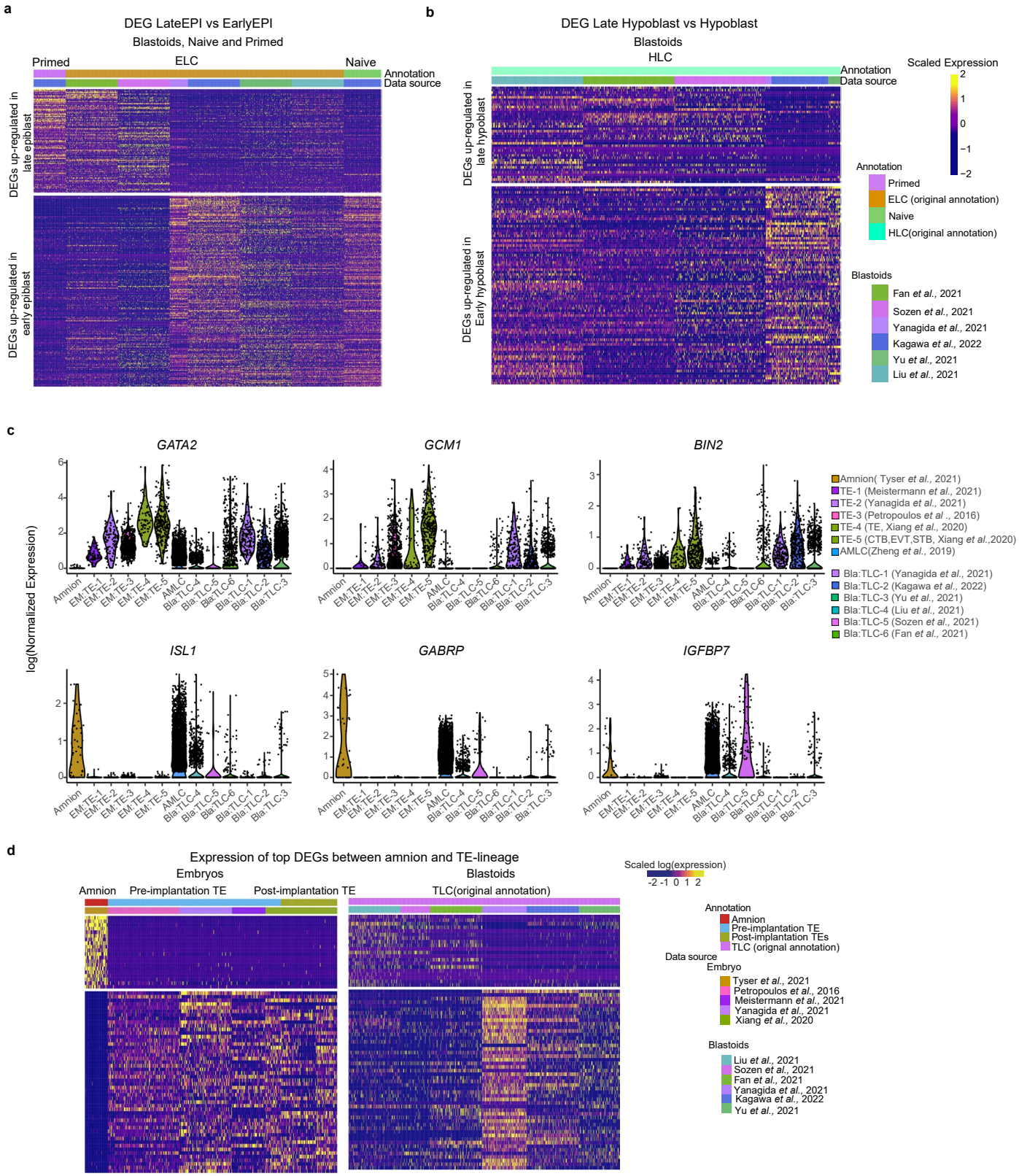

Extended Data Fig. 8 | DEG between cell models and embryo cells. a, Heatmap displaying DEGs between early and late epiblast in primed cells, blastoids ELC cells (based on their original annotation), and naïve cells. **b**, Heatmap displaying DEGs between early and late hypoblast blastoids HLC cells (based on their original annotation). **c**, Violin plots showing log-transformed expression of key amnion and TE markers in amnion, TE, amnion-like cells (AMLC), and TLC from the six blastoids (based on their original annotation). **d**, Expression of DEGs between amnion and TE in embryonic amnion, TE, and TLC from the six blastoid models. For visualisation, cell types containing a large number of cells were randomly down-sampled to 200.

https://doi.org/10.1038/s41592-024-02493-2

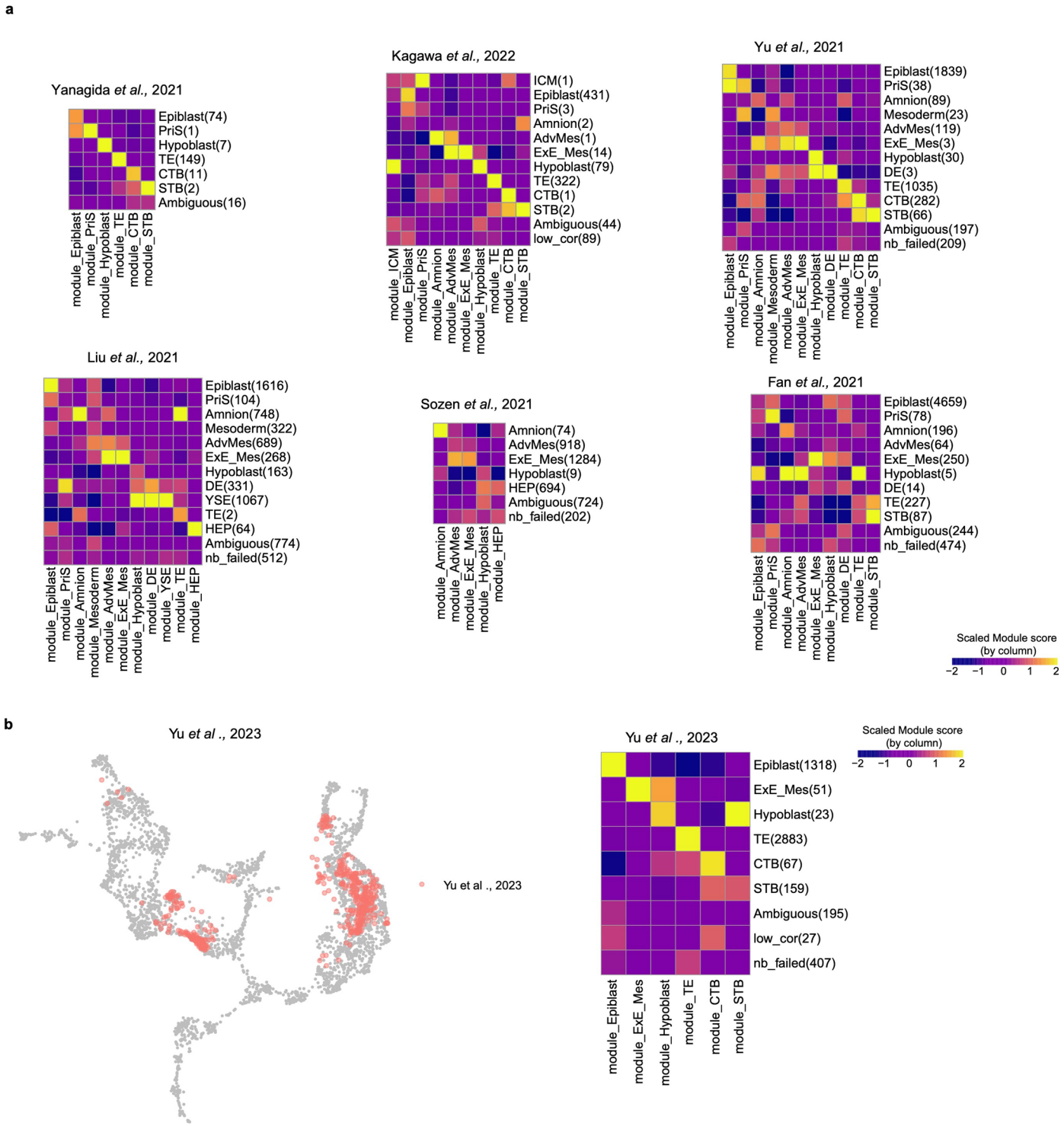

Extended Data Fig. 9 | Module score validation of predicted lineages. **a**, Module score of corresponding predicted lineages in six blastoids. Columns represent different lineage models scores, and rows represent predicted lineages for each dataset. The predicted cell numbers are included in parentheses. **b**, Projection of most-recent blastoids from Yu et al., 2023 onto the human embryonic reference.

https://doi.org/10.1038/s41592-024-02493-2

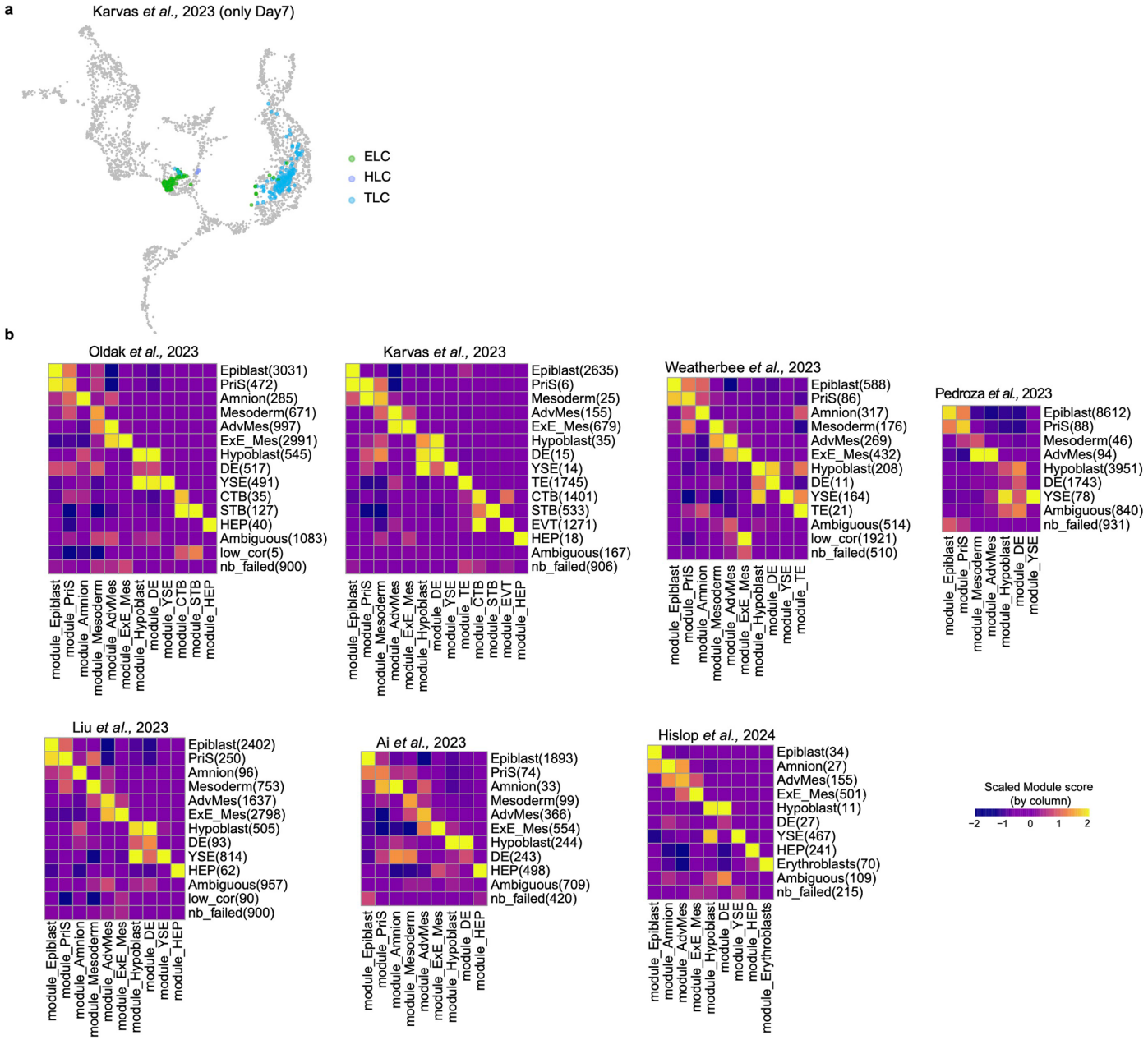

c

	Oldak *et al.*,	Karvas *et al.*,	Weatherbee *et al.*,	Pedroza *et al.*,	Liu *et al.*,	Ai *et al.*,	Hislop *et al.*,
Late Epiblast	+	+	+	+	+	+	+
Primitive streak	+	+	+	+	+	+	-
AdvMes/Mesoderm	+	+	+	+	+	+	+
Amnion	+	-*1	+	-*2	+	+	+
ExE Mes	+	+	+	-	+	+	+
Late_Hypoblast	+	+	+	+	+	+	+
DE	+	-	+	+	+	+	+
YSE	+	+	+	+	+	-	+
TE/CTB	+	+	+	-	-	-	-
STB	+	+	-	-	-	-	-
EVT	-	+	-	-	-	-	-

Note*1:Less than 20 amnion-like cells in original report
Note*2: fewer amnion-like cells than reported

Extended Data Fig. 10 | Analysis of post-implantation models. a, Highlighted cells from the Day 7 blastoids (neighbourhood nodes) from Kavas et al., 2023. The colour of each data point represents the cell annotations retrieved from original publication. **b**, Module score of corresponding predicted lineages in seven post-implantation models. **c**, Presence of post-implantation lineage-like cells in post-implantation embryo models.

nature portfolio

Corresponding author(s): Fredrik Lanner, Sophie Petropoulos

Last updated by author(s): Aug 4, 2024

Reporting Summary

Nature Portfolio wishes to improve the reproducibility of the work that we publish. This form provides structure for consistency and transparency in reporting. For further information on Nature Portfolio policies, see our Editorial Policies and the Editorial Policy Checklist.

Statistics

For all statistical analyses, confirm that the following items are present in the figure legend, table legend, main text, or Methods section.

n/a	Confirmed	
☐	☒	The exact sample size (*n*) for each experimental group/condition, given as a discrete number and unit of measurement
☐	☒	A statement on whether measurements were taken from distinct samples or whether the same sample was measured repeatedly
☐	☒	The statistical test(s) used AND whether they are one- or two-sided *Only common tests should be described solely by name; describe more complex techniques in the Methods section.*
☒	☐	A description of all covariates tested
☐	☒	A description of any assumptions or corrections, such as tests of normality and adjustment for multiple comparisons
☐	☒	A full description of the statistical parameters including central tendency (e.g. means) or other basic estimates (e.g. regression coefficient) AND variation (e.g. standard deviation) or associated estimates of uncertainty (e.g. confidence intervals)
☐	☒	For null hypothesis testing, the test statistic (e.g. *F*, *t*, *r*) with confidence intervals, effect sizes, degrees of freedom and *P* value noted *Give P values as exact values whenever suitable.*
☒	☐	For Bayesian analysis, information on the choice of priors and Markov chain Monte Carlo settings
☒	☐	For hierarchical and complex designs, identification of the appropriate level for tests and full reporting of outcomes
☐	☒	Estimates of effect sizes (e.g. Cohen's *d*, Pearson's *r*), indicating how they were calculated

Our web collection on statistics for biologists contains articles on many of the points above.

Software and code

Policy information about availability of computer code

Data collection	no software except "wget" command was used for data collection
Data analysis	The following software was used in this analysis: Cellranger (v3.0.0 and v6.1.1) was used to process 10X scRNA-seq data. STAR aligner (v2.5.3b) and RSEM (v1.3.0) were employed to map Smart-seq2 scRNA-seq reads. Drop-seq tools (v2.5.1) were used to reprocess data from Ma et al., 2019 (PMID: 31672918). The Seurat R package (v4.2.0) was utilized for scRNA-seq analysis. The Leiden algorithm was applied to identify cell clusters for the human embryonic reference. The scran R package (v1.14.6) was used for normalization. The batchelor R package (v1.2.4) was employed for normalization and integration. The uwot R package (v0.1.14) (https://CRAN.R-project.org/package=uwot) was used to compute the UMAP model. The slingshot R package (v2.6.0) and the SCP R package (v0.5.6, available at https://github.com/zhanghao-njmu/SCP) were used to infer trajectories and identify trajectory-related genes. The poolr R package (v1.1-1) was utilized to merge p-values. The SeuratWrappers R package (v0.3.0) was used for data integration. The miloR R package (v1.2.0) was used to calculate neighborhoods. The caret (v6.0-88) and e1071 (v1.7-13) R packages were used to train SVM models and make predictions. SingleR (v1.4.1), scmap (v1.12.0), and ScType (v6db9eef) were used to compare the prediction performance The ShinyCell R package (v2.1.0) was used to build the Shiny website. The clusterProfiler R package (v3.18.1) was employed to perform gene set enrichment analysis.

Early Embryogenesis Prediction Tool can be browsed at http://petropoulos-lanner-labs.clintec.ki.se

Custom code is available at https://zenodo.org/records/12189592.

For manuscripts utilizing custom algorithms or software that are central to the research but not yet described in published literature, software must be made available to editors and reviewers. We strongly encourage code deposition in a community repository (e.g. GitHub). See the Nature Portfolio guidelines for submitting code & software for further information.

Data

Policy information about availability of data

All manuscripts must include a data availability statement. This statement should provide the following information, where applicable:

- Accession codes, unique identifiers, or web links for publicly available datasets
- A description of any restrictions on data availability
- For clinical datasets or third party data, please ensure that the statement adheres to our policy

Datasets utilised in this study were obtained as summarised in Supplementary Data 9. These include thirteen human embryonic datasets covering various stages of embryogenesis (Yan et al. 2013(GSE36552, https://www.ncbi.nlm.nih.gov/geo/query/acc.cgi?acc=GSE36552); Xiang et al. 2020(GSE136447, https://www.ncbi.nlm.nih.gov/geo/query/acc.cgi?acc=GSE136447); Tyser et al. 2021(E-MTAB-9388, https://www.ebi.ac.uk/arrayexpress/experiments/E-MTAB-9388); Yanagida et al. 2021(GSE171820, https://www.ncbi.nlm.nih.gov/geo/query/acc.cgi?acc=GSE171820); Meistermann et al. 2021(PRJEB30442, https://www.ebi.ac.uk/ena/browser/view/PRJEB30442); Zhou et al. 2019(GSE109555, https://www.ncbi.nlm.nih.gov/geo/query/acc.cgi?acc=GSE109555); Xue et al. 2013(GSE44183, https://www.ncbi.nlm.nih.gov/geo/query/acc.cgi?acc=GSE44183); Molè et al. 2021(E-MTAB-8060, https://www.ebi.ac.uk/arrayexpress/experiments/E-MTAB-8060); Ai et al. 2023(PRJCA017779, https://ngdc.cncb.ac.cn/bioproject/browse/PRJCA017779); Blakeley et al. 2015(GSE66507, https://www.ncbi.nlm.nih.gov/geo/query/acc.cgi?acc=GSE66507); Petropoulos et al. 2016(E-MTAB-3929, https://www.ebi.ac.uk/arrayexpress/experiments/E-MTAB-3929); Xiao et al. 2024(HRA005567, https://ngdc.cncb.ac.cn/gsa-human/browse/HRA005567); Vento-Tormo et al. 2018(E-MTAB-6701, https://www.ebi.ac.uk/arrayexpress/experiments/E-MTAB-6701)). Additionally, we included seven preimplantation blastoid models(Yu et al. 2021 (GSE150578, https://www.ncbi.nlm.nih.gov/geo/query/acc.cgi?acc=GSE150578); Liu et al. 2021(GSE156596, https://www.ncbi.nlm.nih.gov/geo/query/acc.cgi?acc=GSE156596); Kagawa et al. 2022(GSE177689, https://www.ncbi.nlm.nih.gov/geo/query/acc.cgi?acc=GSE177689); Fan et al. 2021(GSE158971, https://www.ncbi.nlm.nih.gov/geo/query/acc.cgi?acc=GSE158971); Sozen et al. 2021(GSE178326, https://www.ncbi.nlm.nih.gov/geo/query/acc.cgi?acc=GSE178326); Yu et al. 2023(GSE210962, https://www.ncbi.nlm.nih.gov/geo/query/acc.cgi?acc=GSE210962); Yanagida et al. 2021(GSE171820, https://www.ncbi.nlm.nih.gov/geo/query/acc.cgi?acc=GSE171820)), seven post-implantation stem cell based models(Karvas et al. 2023(GSE226794, https://www.ncbi.nlm.nih.gov/geo/query/acc.cgi?acc=GSE226794); Hislop et al. 2024(GSE247111, https://www.ncbi.nlm.nih.gov/geo/query/acc.cgi?acc=GSE247111); Weatherbee et al. 2023(GSE218314, https://www.ncbi.nlm.nih.gov/geo/query/acc.cgi?acc=GSE218314); Oldak et al. 2023(GSE239932, https://www.ncbi.nlm.nih.gov/geo/query/acc.cgi?acc=GSE239932); Pedroza et al. 2023(GSE208195, https://www.ncbi.nlm.nih.gov/geo/query/acc.cgi?acc=GSE208195); Liu et al. 2023(GSE232861, https://www.ncbi.nlm.nih.gov/geo/query/acc.cgi?acc=GSE232861); Ai et al. 2023(PRJCA017779, https://ngdc.cncb.ac.cn/bioproject/browse/PRJCA017779)), three studies involving naïve cells giving rise to trophectoderm (TE)-like cells(Io et al. 2021(GSE167924, https://www.ncbi.nlm.nih.gov/geo/query/acc.cgi?acc=GSE167924); Guo et al. 2021(GSE166422, https://www.ncbi.nlm.nih.gov/geo/query/acc.cgi?acc=GSE166422); Osnato et al. 2021(E-MTAB-10018, https://www.ebi.ac.uk/arrayexpress/experiments/E-MTAB-10018)), three studies using primed human embryonic cells giving rise to TE-like cells (one generated in house(GSE254641, https://www.ncbi.nlm.nih.gov/geo/query/acc.cgi?acc=GSE254641) ,Soncin et al. 2022(GSE182791, https://www.ncbi.nlm.nih.gov/geo/query/acc.cgi?acc=GSE182791); Ohgushi et al. 2022(GSE196365, https://www.ncbi.nlm.nih.gov/geo/query/acc.cgi?acc=GSE196365)), two studies analysing 8-cell-like cells(Mazid et al. 2022(CNP0001454, https://db.cngb.org/search/project/CNP0001454/); Yoshihara et al. 2022(E-MTAB-10581, https://www.ebi.ac.uk/arrayexpress/experiments/E-MTAB-10581)), one study with a post-implantation amniotic sac embryoid (PASE)-model(Zheng et al. 2019(GSE134571, https://www.ncbi.nlm.nih.gov/geo/query/acc.cgi?acc=GSE134571)), and one study from human trophoblast organoids(Shannon et al. 2024(GSE216244, https://www.ncbi.nlm.nih.gov/geo/query/acc.cgi?acc=GSE216244)). Furthermore, we included two embryonic datasets from Callithrix jacchus (marmoset)(Bergmann et al. 2022(E-MTAB-9367, https://www.ebi.ac.uk/biostudies/arrayexpress/studies/E-MTAB-9367); Boroviak et al. 2018(E-MTAB-7078, https://www.ebi.ac.uk/arrayexpress/experiments/E-MTAB-7078)) and three embryonic datasets from Macaca fascicularis (Crab-eating macaque)(Nakamura et al. 2016(GSE74767, https://www.ncbi.nlm.nih.gov/geo/query/acc.cgi?acc=GSE74767); Ma et al. 2019(GSE130114, https://www.ncbi.nlm.nih.gov/geo/query/acc.cgi?acc=GSE130114); Yang et al. 2021(GSE148683, https://www.ncbi.nlm.nih.gov/geo/query/acc.cgi?acc=GSE148683)).

WikiPathway annotations and gene sets for GSEA analysis were downloaded from the Molecular Signatures Database (https://www.gsea-msigdb.org/gsea/msigdb) The processed dataset with predicted annotations, projected UMAP, and sorted cell counts, can be retrieved from https://petropoulos-lanner-labs.clintec.ki.se/dataset.download.html.

Early Embryogenesis Prediction Tool can be browsed at http://petropoulos-lanner-labs.clintec.ki.se

Human research participants

Policy information about studies involving human research participants and Sex and Gender in Research.

Reporting on sex and gender	NA
Population characteristics	NA
Recruitment	NA
Ethics oversight	NA

Note that full information on the approval of the study protocol must also be provided in the manuscript.

Field-specific reporting

Please select the one below that is the best fit for your research. If you are not sure, read the appropriate sections before making your selection.

☒ Life sciences ☐ Behavioural & social sciences ☐ Ecological, evolutionary & environmental sciences

For a reference copy of the document with all sections, see nature.com/documents/nr-reporting-summary-flat.pdf

Life sciences study design

All studies must disclose on these points even when the disclosure is negative.

Sample size	We included 42 datasets because they're relevent with this study.
Data exclusions	No data were excluded from the analyses, except that cells with unknown annotation were excluded from visualization in Fig. 1a and Extended Data Fig. 3a.
Replication	The biological replication is represented by the samples included in the datasets.
Randomization	Based on prediciton performance, downsampling sample size in Fig.2a were determined as 200. No data were excluded from the analyses. The samples were not randomized unless specified in Extended Data Fig. 3a, d and Extended Data Fig. 8a, b and d. Cells from Yang et al., 2021 were downsampled to 2000 in Extended Data Fig. 3a. Cells more than 200 cells were downsampled to 200 in Extended Data Fig. 3d and Extended Data Fig. 8a, b and d.
Blinding	Datasets were processed without taking group allocation into account.

Reporting for specific materials, systems and methods

We require information from authors about some types of materials, experimental systems and methods used in many studies. Here, indicate whether each material, system or method listed is relevant to your study. If you are not sure if a list item applies to your research, read the appropriate section before selecting a response.

Materials & experimental systems

n/a	Involved in the study
☒	☐ Antibodies
☐	☒ Eukaryotic cell lines
☒	☐ Palaeontology and archaeology
☒	☐ Animals and other organisms
☒	☐ Clinical data
☒	☐ Dual use research of concern

Methods

n/a	Involved in the study
☒	☐ ChIP-seq
☒	☐ Flow cytometry
☒	☐ MRI-based neuroimaging

Eukaryotic cell lines

Policy information about cell lines and Sex and Gender in Research

Cell line source(s)	Human embryonic stem cell line hs975 (KIe032-A in hPSC-reg database) was derived at Karolinska Institutet, described in Rodin S et al. Clonal culturing of human embryonic stem cells on laminin-521/E-cadherin matrix in defined and xeno-free environment. Nature communications. 2014;5:3195.
Authentication	Express pluripotency markers POU5F1 and NANOG. Trilineage differentiation has been performed.
Mycoplasma contamination	The cell line is regularly tested for mycoplasma and is indeed negative.
Commonly misidentified lines (See ICLAC register)	Not applicable